Strål säkerhets myndigheten
Swedish Radiation Safety Authority

Author: Digby D. Macdonald
Feixiong Mao
Chaofang Dong
Samin Sharifi-Asl

Research

2016:30

Measurement of Parameter Values for Predicting Corrosion Phenomena on Copper in Swedish HLNW Repositories

Phase IV: Impact of Chloride Ion on the Passivity and Pitting of Copper

Report number: 2016:30 **ISSN:** 2000-0456
Available at www.stralsakerhetsmyndigheten.se

SSM perspektiv

Bakgrund

I Sverige planeras slutförvaringen av det använda kärnbränslet. Metoden som har utvecklats kallas för KBS-3 och bygger på tre skyddsbarriärer: kopparkapslar, bentonitlera och det svenska urberget. I den aktuella KBS-3-utformningen kommer det använda kärnbränslet placeras i en insats av gjutjärn inuti en 50 mm tjock kopparkapsel. Den ska sedan deponeras i ett kristallint bergförvar planerat i Forsmark på ett djup på ca 500 m. Gjutjärnsinsatsen ger mekanisk hållfasthet och strålskydd, medan kopparkapselns roll är att förebygga korrosion. I utvärderingen av KBS-3-systemet är förståelsen för långtidsutveckling av processer som kan påverka kapseln, inklusive lokal degradering till exempel via gropfrätning, mycket viktig.

Det nuvarande forskningsarbetet (fas IV) är en fortsättning av de forskningsprojekt som utfördes i fas I-III. Det syftar till att ge en bättre och noggrannare definition av de förutsättningar som kan leda till att gropfrätning förekommer i förvaret under den planerade förvaringsperioden på mer än 100 000 år. Projektet har koncentrerat sig på att utvärdera effekterna av kloridhalterna, pH och temperatur på passiviteten av koppar i sulfidhaltiga saltlösningar och karakterisera hur känslig koppar kan vara mot gropfrätning i dessa miljöer.

Projektets syfte

Syftet med detta forskningsprojekt har varit att göra fullständiga mätningar av parametrarna som behövs för ”mixed potential model” (MPM). Det kommer att användas för att uppskatta redoxpotentialen i slutförvaret samt korrosionspotentialen och korrosionshastigheten av kopparkapseln över hela den ”korrosionsevolutionära utvecklingen” (CEP) av förvaret. Undersökningarna inkluderade följande:

- Undersökning av de elektroniska egenskaperna hos den passiva filmen av sulfid som bildas på kopparytan.
- Mätning av parametrar som igår i Punkt Defekt Modellen, PDM, för bildandet av Cu_2S.
- Mätning av upplösningshastigheten för den passiva Cu_2S-filmen på kopparytan.
- Mätning av kinetiska parametrar för utvecklingen av väte från korrosion av koppar.
- Fortsätta utveckla Mixed Potential-modellen.
- Implementering av parametervärdena i Mixed potential-modellen.
- Prediktering av redoxpotentialen, korrosionspotentialen, korrosionshastigheten och korrosionsrelaterad degradering över hela den ”korrosionsevolutionära utvecklingen” (CEP) av förvaret.

Med hjälp av mera avancerade fysikaliska-elektrokemiska modeller har det även blivit möjligt att jämföra korrosionspotentialen och korrosionshastigheten för kopparkapseln med SKB:s senaste resultat.

Författarnas sammanfattning
Passivitet-nedbrytning och gropfrätning av koppar i kapselmaterialet som har valts av SKB för inneslutning av högaktivt kärnavfall i Sverige, har studerats i detta projekt med ett simulerat sulfid och kloridinnehållande grundvatten. Uppgifterna har även analyserats med Punkt Defekt Modellen (PDM). Resultaten indikerar på att ett sulfidbaserat barriärskikt kan bildas på kopparytan, och att kloridjonerna kan inducera passivitetsnedbrytning och därmed inducera utvecklingen av lokal degradering via korrosion (LCD), såsom gropfrätning, på kapselytan. I denna studie har effekterna av olika parametrar, som kloridkoncentration (0,01–5 M), lösningens pH (= 8–10) och temperatur (22–82°C), undersökts för att öka kunskapen på initiering och propagering av gropfrätning i koppar i simulerade grundvatten som är relevant för slutförvaret. En mera detaljerad sammanfattning av forskningsprojektets resultat återfinns i författarnas sammanfattning i avsnittet "Executive Summery".

Projekt information
Kontaktperson på SSM: Bo Strömberg
Diarienummer: SSM2014-282
Aktivitetsnummer: 3030045-09

SSM perspective

Background

The Swedish plan for disposal of High-Level Nuclear Waste (HLNW) implies the encapsulation of spent fuels and deposition of the canisters holding the spent fuel in a crystalline bedrock repository at a depth of about 500 m. In the current KBS-3 design, the spent fuel will be emplaced in an inner cast iron insert that is contained in a copper canister with a 50 mm wall thickness. The role of the cast iron insert is to provide mechanical strength as well as radiation shielding, while the copper canister's (the outer layer) role is to provide corrosion protection, thus for the evaluation of the performance of the KBS-3 system, understanding of the long-term development of the processes that can affect the canister including local degradation via corrosion for example by pitting corrosion is very important.

The proposed work (Phase IV) is a continuation of work performed in the research projects from Phases I - III in order to provide a better and more accurate definition of the conditions that could influence the pitting corrosion of copper canister as the repository evolves over the planned storage period of more than 100,000 years. The project has concentrated on evaluating the impact of chloride ion, pH, and temperature on the passivity of copper in sulphide-containing brines and in characterizing the susceptibility of copper to pitting corrosion in these environments.

Objective

The objectives of the proposed research work have been to measure the full slate of parameters for the mixed potential models (MPMs) that was then used to estimate the redox potential of the repository, corrosion potential and the corrosion rate of the copper canister in the repository over the Corrosion Evolutionary Path (CEP). These measurements included the following:

- Determination of Electronic Character of Cu_2S on Cu.
- Measurement of Values for Parameters in the Point Defect Model, PDM, for the formation of Cu_2S.
- Measurement of the Dissolution Rate of the Passive Cu_2S film on Copper.
- Measurement of Kinetic Parameters for the Evolution of Hydrogen on Copper.
- Continued Development of the Mixed Potential Models.
- Insertion of the Parameter Values into the Mixed Potential Models.
- Prediction of the Redox Potential, Corrosion Potential, Corrosion Rate, and Corrosion damage over the Corrosion Evolutionary Path.

Using more advanced physico-electrochemical models, the corrosion potential and the corrosion rate for the copper canister have been calculated and the results compared with those predicted by SKB in their modeling program.

Summary by the authors
Passivity breakdown and pitting on pure copper, the assumed material for the canisters for the isolation of high-level nuclear waste in Sweden, has been studied in simulated, sulphide- and chloride containing granitic rock groundwater and the data are interpreted in terms of the Point Defect Model (PDM). The results indicated that a sulphide barrier layer forms on the copper surface, and that chloride ion can induce passivity breakdown, and hence induce the development of localized corrosion damage (LCD), such as pitting corrosion, on the canister surface. In this study, the effects of chloride concentration (0.01–5 M), solution pH (= 8–10), and temperature (22–82°C) on the pitting corrosion of copper in simulated repository ground water have been studied. The principal findings of the study are summarized in the executive summary written by the authors.

Project information
Contact person SSM: Bo Strömberg
Reference number: SSM2014-282
Activity number: 3030045-09

Strål
säkerhets
myndigheten
Swedish Radiation Safety Authority

Authors: Digby D. Macdonald[1], Feixiong Mao[1, 2]
Chaofang Dong[1, 3], Samin Sharifi-Asl[1]

[1] Department of Materials Science and Engineering
The University of California at Berkeley,
Berkeley, CA 94720

[2] School of Materials and Metallurgy
Northeastern University
Shenyang 110819, China

[3] Corrosion and Protection Center
The University of Science and Technology Beijing,
Beijing 100083, China

2016:30

Measurement of Parameter Values for Predicting Corrosion Phenomena on Copper in Swedish HLNW Repositories

Phase IV: Impact of Chloride Ion on the Passivity and Pitting of Copper

Date: September 2016
Report number: 2016:30 **ISSN:** 2000-0456
Available at www.stralsakerhetsmyndigheten.se

This report concerns a study which has been conducted for the Swedish Radiation Safety Authority, SSM. The conclusions and viewpoints presented in the report are those of the author/authors and do not necessarily coincide with those of the SSM.

Contents

1. Executive Summary

Passivity breakdown and pitting on pure copper, the assumed material for the canisters for the isolation of high-level nuclear waste in Sweden, has been studied in simulated, sulphide- and chloride-containing granitic rock groundwater and the data are interpreted in terms of the Point Defect Model (PDM). The results indicated that a sulphide barrier layer forms on the copper surface, and that chloride ion can induce passivity breakdown, and hence induce the development of localized corrosion damage (LCD), such as pitting corrosion, on the canister surface. In this study, the effects of chloride concentration (0.01 – 5 M), solution pH (= 8-10), and temperature (22 - 82ºC) on the pitting corrosion of copper in simulated repository ground water have been studied. The principal findings of the study are as follows:

- Pitting corrosion is observed on copper at elevated temperatures in simulated sulphide- and chloride-containing granitic rock groundwater where cuprous sulphide (Cu_2S) comprises the barrier layer of the passive film. The results show that increasing temperature decreases the mean breakdown potential.
- Experimental relationships between the breakdown potential (V_c) and chloride activity and pH have demonstrated the validity of the Point Defect Model (PDM) for describing passivity breakdown on copper in chloride-containing sodium sulphide solutions.
- Experimental relationships between the breakdown potential (V_c) and temperature are readily accounted for by the Point Defect Model (PDM) for describing passivity breakdown on copper in chloride-containing sodium sulphide solutions. Analysis of the dependence of the breakdown potential on chloride concentration yields the value for the polarizability (α = 0.52 – 0.54) of the barrier layer/solution interface at different temperatures.
- The dependence of the breakdown voltage on pH at constant [Cl^-] yields a value of -0.0109V for the dependence of the potential drop across the film/solution, f/s, interface on the applied voltage, β. This value is similar to that measured for passivity breakdown of oxide barrier layers.
- Metastable pitting events, which appear as “spikes” on the polarization curve, are observed at potentials that are more than 500 mV more negative than the critical breakdown voltage. Should one or more of these pit nuclei stabilize via the establishment of differential aeration, then stable pitting will result and cause macroscopic damage to the canister.

- The critical areal cation vacancy concentration ξ leading to passivity breakdown on copper is of the order of 1.09×10^{15} cm^{-2}, as determined from the dependence of the apparent breakdown potential on the potential sweep rate, as given by the PDM. This is in excellent agreement with that (10^{14} -10^{15} cm^{-2}) estimated structurally, assuming vacancy condensation on either the copper substrate or on the cation sublattice of the barrier layer (Cu_2S).
- The critical, areal cation vacancy concentration, ξ, leading to passivity breakdown on copper is in the range of 1.04×10^{15} - $1.14\times10^{15}cm^{-2}$ when the temperature changes from 42 ℃ to 82 ℃, as determined from the dependence of the apparent breakdown potential on the potential sweep rate, as given by the PDM. These values are in excellent agreement with that (10^{14} - $10^{15}cm^{-2}$) estimated structurally, assuming vacancy condensate ion on either the copper substrate or on the cation sub-lattice of the barrier layer (Cu_2S).
- The experimentally-determined, near normal distributions in the cumulative probability of the breakdown potential for different chloride concentrations are found to be in satisfactory agreement with theory in the quantitative characterization of the breakdown potential distributions for Cu as calculated from the PDM. Because the CPD approaches the abscissa asymptotically as the potential is reduced, there exists a finite probability that passivity breakdown might occur at a potential that is considerably more negative (perhaps by 200 or 300 mV) than the mean breakdown voltage, particularly in the light of the large surface area of a canister and the excessively long exposure time in the repository. Such breakdown sites would be characterized by abnormally high cation vacancy diffusivities.
- The experimentally-determined, near normal distributions in the breakdown potential for different temperatures are found to be in satisfactory agreement with theory in the quantitative characterization of the breakdown potential distributions for Cu as predicted from the PDM.
- Preliminary analysis shows that conditions that will be conducive to passivity breakdown and possibly stable pitting will exist within the repository, particularly during the thermal phase and if the chloride concentration is high. In general, the pitting potential shifts to more negative values (pitting becomes more prevalent) with increasing [Cl^-] and with increasing temperature.
- Preliminary measurements have been made of the maximum pit depth from which the pitting factor is estimated, knowing the passive current density, and hence the general corrosion loss, just prior to pit nucleation. The passive current density is

used to estimate the general corrosion metal loss using Faraday's law. The pitting factor (PF) is found to decrease exponentially with time, but it eventually levels off to a value between 4 and 14, depending upon the temperature (the PF is larger at higher temperatures). The maximum pit depth is found to approach a constant value with increasing time, as has been observed for many other systems, but the observation times were very short compared with the repository storage time, so that not too much significance must be read into these preliminary observations. However, they do illuminate the path that must be taken in future studies.

- We also report preliminary measurements of the repassivation potential and this parameter is found to decrease significantly with increasing charge passed during pit growth. We stress, however, that these pits are very shallow compared with those that may develop over the much longer times that will exist in the repository. The repassivation potential is expected to shift in the negative direction with increasing pit depth, such that a lower tendency will exist for active pits to die and the accumulation of localized corrosion damage to cease spontaneously.
- The pitting potential has been estimated for various times along the corrosion evolutionary path out to a horizon of 10,000 years by combining the predicted change in temperature with the dependence of the pitting potential as a function of temperature as measured in this work. The pitting potential is predicted to shift slightly in the negative direction (pitting becomes easier) during the initial heat-up of the repository followed by a long trend to more positive values (pitting becomes more difficult) as the temperature declines.

We conclude from this work that pitting corrosion can occur, particularly at high chloride concentration, low pH, and high temperature, all of which displace the critical breakdown voltage in the negative direction, thereby rendering the metal more susceptible to pitting corrosion. The critical issue is that, although the corrosion potential is estimated to lie below the mean critical breakdown voltage over much of the corrosion evolutionary path of the canister in the repository, as currently defined, the cumulative distribution function in the breakdown potential approaches the axis asymptotically, so that even at very low potentials the probability of pit nucleation is not zero, corresponding to the existence of potential breakdown sites on the surface that are characterized by high cation vacancy diffusivity. Given the length of the storage period (10^5 to 10^6 years), and the large population of breakdown sites on the metal surface, the probability that pits will nucleate on the surface is judged to be high. However,

any pits that do nucleate will die if the corrosion potential drops below the repassivation potential, which is only about 50mV more negative than the mean critical breakdown voltage, as measured for very shallow, naturally-grown pits, suggesting that any stable pit that grows will quickly repassivate, but the data required to arrive at an unequivocal conclusion on this issue are currently not available. It is our recommendation that this issue be explored within the framework of Damage Function Analysis (DFA), particularly by applying Deterministic Extreme Value Statistics (DEVS). As a consequence we outline a program of research that will extend the science and technology forward and which will provide unequivocal resolution of these important issues.

2. Introduction

2.1. Background

The KBS-3 repository concept developed by SKB for disposal of spent nuclear fuel in Sweden is based on the multi barrier concept for isolating the fuel and delaying any escaping radionuclides from reaching the biosphere within the intended storage period (10^5 to 10^6 years). The concept is based on the presence of at least four engineered barriers; the fuel sheathing, the copper canister, the bentonite buffer, and the granitic bedrock. The copper canister will, in this respect, represent an important corrosion barrier and is intended to completely isolate the spent nuclear fuel from the surroundings until failure occurs of the 5 cm thick copper canister by either corrosion or mechanical loading.

The three previous phases of this research program were concerned with characterizing the chemical conditions that are likely to exist in the crystalline rock repository and with characterizing the passive state on copper in sulphide-containing ground water. The results of Phases I through III have been presented in annual reports to SSM. In Phase IV, which was performed in 2014, our research concentrated on the impact of chloride ion, pH, and temperature on the passivity of copper in sulphide-containing brines and in characterizing the susceptibility of copper to pitting corrosion in the same environments.

It has been reported by Shoesmith et.al. [1], under sponsorship of SKB, that the Cu_2S passive film that forms on copper in contact with sulphide-containing NaCl brine becomes very porous at high [Cl^-]. If so, this could have a dramatic effect on the corrosion resistance of copper in the proposed Swedish repository for the isolation of HLNW. In this regard, it is important to note that Cl^-, unlike HS^-, is likely not consumed at the canister surface and hence its presence at the copper surface is not transport-controlled by the buffer. In other words, as far as Cl^- is concerned, the bentonite barrier does not act as an "engineered barrier", unless chloride is consumed via the formation of CuCl, for example. Consumption of Cl^- by CuCl formation is unlikely, however, because the solubility of Cu_2S is very much lower than that of CuCl, indicating the precipitation of the sulphide will reduce the Cu^+ concentration to below that at which CuCl will precipitate for the prevailing chloride concentration. This is an important point, because it can be argued that, as far as general corrosion is concerned (i.e., due to the formation of Cu_2S), the rate of copper corrosion is ultimately limited by the rate of transport of HS^-

through the buffer and hence if the transport rate is rendered sufficiently small, the corrosion rate of the canister will also be acceptably small. In our previous work on the passivity of copper in simulated granitic ground water, we employed only a single [Cl^-] of 0.1 M, which is well below the concentration of 1.0 M reported by Shoesmith et.al. as being the threshold for the formation of the porous passive film. In the work reported here, we have extended our previous experimental studies of the passivity of copper in simulated granitic ground water [2] to 0.1M < [Cl^-] < 5 M. Our experimental work employed potentiodynamic and potentiostatic polarization techniques, surface analysis (optical microscopy, scanning electron microscopy), and wide-band electrochemical impedance spectroscopy (WBEIS), which upon optimization of the Point Defect Model (PDM), as described in our 2013 Annual Report [2], provides quantitative information on the porosity of the passive film as well as on the passive current density (a measure of the copper corrosion rate) as a function of potential, pH, temperature, and [Cl^-].

That copper suffers pitting corrosion in sulphide-containing brine is indicated by the potentiodynamic polarization curves plotted in Figure 1.1, which we reported in our Phase III work [2]. Thus, one sees typical passivity breakdown phenomena at high potentials, in which the current increases sharply as breakdown occur. The apparent breakdown voltages, V_c, are approximately 0.2 V_{SHE}, 0.1 V_{SHE} and 0V_{SHE} for chloride concentrations of 0.01, 0.1, and 0.5 M, respectively. However, we have shown theoretically, and have demonstrated experimentally, that the critical breakdown voltage is a near-normally distributed quantity and that each experiment must be repeated at least 20 times, in order to define the distribution. The importance of this is that, even if the corrosion potential is lower (more negative) than the mean in the distribution in V_c, a finite probability of pitting exists, with the probability increasing with increasing exposure time, which for HLNW canisters in repositories is extreme (> 100,000 years), and because of the very large surface area of the canister. Thus, the Phase IV work yields the distribution in the critical breakdown potential as a function of [Cl^-], pH, and temperature, and hence enables us to assess the likelihood of pitting corrosion on copper as a function of chloride concentration at any point along the corrosion evolutionary path (CEP) that describes the evolution of the repository in terms of those parameters that significantly affect the damage accumulation rate, by interpreting the results in terms of the Point Defect Model [3].

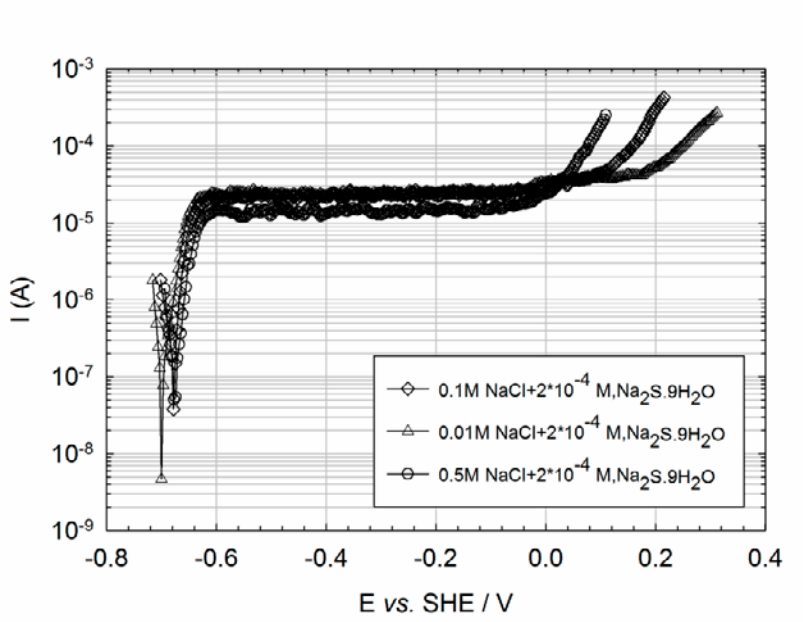

Figure 1.1. Potentiodynamic polarization curves of Cu in a deaerated NaCl+2×10^{-4} M $Na_2S.9H_2O$ solution at ambient temperature (25°C) as a function of chloride concentration. (Scan rate=1 mV s^{-1}) [2].

2.2. Point defect model

The anodic processes that occur on copper in pure, deoxygenated water are a matter of considerable controversy, with Hultqvist et.al. [4-6] claiming that copper corrodes under these conditions, while others insist that the metal is immune. This controversy was resolved in Phase I of this program, where we demonstrated that both positions could be correct depending upon the initial conditions of the experiment, as shown in Figure 1.2.

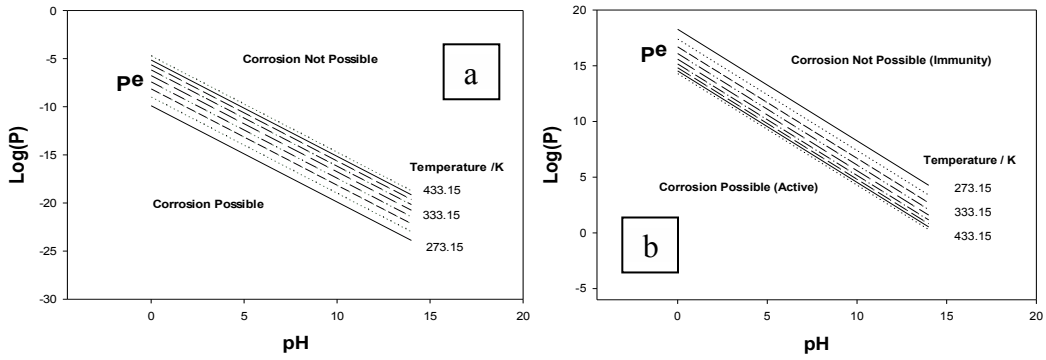

Figure 1.2. Corrosion domain diagram (CDD) for copper in sulphide free, pure water environments (a) and in sulphide-containing aqueous environments (b) [1].

Thus, if the initial value of $P = f_{H_2}^{1/2} a_{Cu^+}$ lies below the equilibrium value (P_e) calculated for the reaction, $Cu + H^+ = Cu^+ + 1/2H_2$ copper will corrode, as reported by Hultquist et.al. [4-6], because the Gibbs energy change (ΔG) is negative, but if $P > P_e$, corrosion cannot occur, because ΔG is positive and hence the metal is immune. In the presence of sulphide, copper corrodes unequivocally under all practical conditions, because of the formation of Cu_2S at a potential that is much more negative than those for Cu/Cu^+ and Cu/Cu_2O. The potential of the Cu/Cu_2S reaction is sufficiently negative that the hydrogen evolution reaction

$$2H_2O + 2e^- \xleftrightarrow{k_2, k_{-2}} 2OH^- + H_2 \qquad (1.1)$$

is thermodynamically viable, according to the criterion derived from the Second Law of Thermodynamics, which states that for a corrosion process to be viable then $E_a^e < E_{corr} < E_c^e$. Here, E_a^e and E_c^e are the equilibrium potentials for the partial anodic and cathodic processes, respectively, and E_{corr} is the corrosion potential. It is evident, therefore, that the partial anodic reaction of interest for copper in sulphide-containing environments is

$$2Cu + HS^- \xrightarrow{k_1} Cu_2S + H^+ + 2e^- \qquad (1.2)$$

What this means, practically, is that any measurable sulphide concentration will result in general corrosion with the formation of a Cu_2S barrier layer, as has been confirmed experimentally. Thus, as far as passivity breakdown and the possibility of localized corrosion (pitting) is concerned, one must inquire into the localized breakdown of a sulphide barrier layer, when only the breakdown of oxide barrier layers have been considered in the past. Thus, the exploration of passivity breakdown of a Cu_2S barrier layer represents a significant departure from the previous studies on this subject.

The Point Defect Model representation of the formation of Cu_2S on copper in sulphide-containing environments is depicted theoretically as [7, 8]:

Metal | Barrier Layer, Cu_2S | Solution/Precipitated Outer Layer

(1) $Cu + V_{Cu}{}' \overset{k_1}{\rightarrow} Cu_{Cu} + v_{Cu} + e^-$ (4) $Cu_{Cu} \overset{k_4}{\rightarrow} Cu_s^+ + V_{Cu}{}'$

(2) $Cu \overset{k_2}{\rightarrow} Cu_i^+ + v_{Cu} + e^-$ (5) $Cu_i^+ \overset{k_5}{\rightarrow} Cu_s^+$

(3) $Cu \overset{k_3}{\rightarrow} Cu_{Cu} + \frac{1}{2}V_S^{\circ\circ} + e^-$ (6) $V_S^{\circ\circ} + HS^- \overset{k_6}{\rightarrow} S_S + H^+$

(7) $CuS_{1/2} + \frac{1}{2}H^+ \overset{k_7}{\rightarrow} Cu^+ + \frac{1}{2}HS^-$

Figure 1.3. Point Defect Model representation for the formation of Cu_2S on copper. Note that the Cu^+ cation, which is transmitted through the barrier layer by cation vacancy movement via Reactions (1) and (4) and/or as interstitials via Reactions (2) and (5), will react with additional HS^- to form the precipitated, outer later with the overall stoichiometry being described by Reaction (1.2).

The rate constants for these reactions have been derived using the method of partial charges and the expressions are summarized in Tables 1.1 and 1.2 [7, 8].

Table 1.1. Rate constants $k_i = k_i^0 e^{a_i V} e^{b_i L} e^{c_i pH}$ for the interfacial defect generation and annihilation reactions employed in the Point Defect Model. $K = \varepsilon\gamma$, $\chi = 1$ (for a Cu_2S barrier layer), and $\gamma = F/RT$.

Reaction	$\boldsymbol{a_i(V^{-1})}$	$\boldsymbol{b_i(cm^{-1})}$	$\mathbf{c_i}$
(1) $Cu + V_{Cu}{}' \overset{k_1}{\rightarrow} Cu_{Cu} + v_{Cu} + e^-$	$\alpha_1(1-\alpha)\chi\gamma$	$-\alpha_1\varepsilon\chi\gamma$	$-\alpha_1\beta\gamma\chi$
(2) $Cu \overset{k_2}{\rightarrow} Cu_i^+ + v_{Cu} + e^-$	$\alpha_2(1-\alpha)\chi\gamma$	$-\alpha_2\varepsilon\chi\gamma$	$-\alpha_2\beta\gamma\chi$
(3) $Cu \overset{k_3}{\rightarrow} Cu_{Cu} + \frac{1}{2}V_S^{\circ\circ} + e^-$	$\alpha_3(1-\alpha)\chi\gamma$	$-\alpha_3\varepsilon\chi\gamma$	$-\alpha_3\beta\gamma\chi$
(4) $Cu_{Cu} \overset{k_4}{\rightarrow} Cu_s^+ + V_{Cu}{}'$	$\alpha_4\alpha\gamma\chi$		$\alpha_4\beta\gamma\chi$
(5) $Cu_i^+ \overset{k_5}{\rightarrow} Cu_s^+$	$\alpha_5\alpha\gamma\chi$		$\alpha_5\beta\gamma\chi$
(6) $V_S^{\circ\circ} + HS^- \overset{k_6}{\rightarrow} S_S + H^+$	$2\alpha_6\alpha\gamma\chi$		$2\alpha_6\beta\gamma\chi$
(7) $CuS_{1/2} + \frac{1}{2}H^+ \overset{k_7}{\rightarrow} Cu^+ + \frac{1}{2}HS^-$	0		0

Table 1.2. Definition of the standard rate constants for the interfacial defect generation and annihilation reactions employed in the Point Defect Model. Note that the base rate constant for the i^{th} reaction is designated k_i^{00}.

Reaction	$\boldsymbol{k_i^0}$
(1) $Cu + V_{Cu}^{1'} \overset{k_1}{\rightarrow} Cu_{Cu} + v_{Cu} + e^-$	$k_1^{00} e^{-\alpha_1 \gamma \varphi_{f/s}^0} e^{\frac{-E_{a,1}}{RT}\left(\frac{1}{T}-\frac{1}{T_0}\right)}$
(2) $Cu \overset{k_2}{\rightarrow} Cu_i^+ + v_{Cu} + e^-$	$k_2^{00} e^{-\alpha_2 \gamma \varphi_{f/s}^0} e^{\frac{-E_{a,2}}{RT}\left(\frac{1}{T}-\frac{1}{T_0}\right)}$
(3) $Cu \overset{k_3}{\rightarrow} Cu_{Cu} + \frac{1}{2}V_S^{\circ\circ} + e^-$	$k_3^{00} e^{-\alpha_3 \gamma \varphi_{f/s}^0} e^{\frac{-E_{a,3}}{RT}\left(\frac{1}{T}-\frac{1}{T_0}\right)}$
(4) $Cu_{Cu} \overset{k_4}{\rightarrow} Cu_s^+ + V_{Cu}^{1'}$	$k_4^{00} e^{-\alpha_4 \gamma \varphi_{f/s}^0} e^{\frac{-E_{a,4}}{RT}\left(\frac{1}{T}-\frac{1}{T_0}\right)}$
(5) $Cu_i^+ \overset{k_5}{\rightarrow} Cu_s^+$	$k_5^{00} e^{\alpha_5 \gamma \varphi_{f/s}^0} e^{\frac{-E_{a,5}}{RT}\left(\frac{1}{T}-\frac{1}{T_0}\right)}$
(6) $V_S^{\circ\circ} + HS^- \overset{k_6}{\rightarrow} S_S + H^+$	$k_6^{00} e^{2\alpha_6 \gamma \varphi_{f/s}^0} e^{\frac{-E_{a,6}}{RT}\left(\frac{1}{T}-\frac{1}{T_0}\right)}$
(7) $CuS_{1/2} + \frac{1}{2}H^+ \overset{k_7}{\rightarrow} Cu^+ + \frac{1}{2}HS^-$	$k_7^{00} e^{\frac{-E_{a,7}}{RT}\left(\frac{1}{T}-\frac{1}{T_0}\right)}$

2.3. Passive breakdown

Sweden's KBS-3 multi-barrier plan for the disposal of high-level nuclear waste (HLNW) was initially, partly predicated on the assumption that copper, the material from which the canisters will be fabricated, is a semi-noble metal when in contact with water, although this view was abandoned when it was recognized that granitic ground water contained significant sulphide ion and from an appreciation of the activating effect of sulphide ion on the corrosion of copper. Thus, the environment within the proposed repositories is not pristine, pure water, but instead is brine containing a variety of species, including halide ions, sulfur-containing species, as well as iron oxidation products. Recognizing that copper metal loses much of its corrosion resistance in the presence of sulphide ion and other sulfur-containing species [9-14], with the metal forming a Cu_2S barrier layer of the passive film, Sharifiasl and Macdonald expanded the Point Defect Model (PDM) [7, 8] representation of a passive film to cover of the formation of Cu_2S barrier layer, which has been described in detail elsewhere [9]. Study of the relationships that exist between the concentrations of aggressive ions and species that determine the identity of the barrier layer (HS^-, S^{2-}) and that result in passivity breakdown (Cl^-), and the critical breakdown potential (V_c) for localized corrosion processes, such as pitting corrosion, is expected to indicate whether localized corrosion damage (LCD) is likely to develop on the copper canisters in the repository.

The initial events in the accumulation of LCD are passivity breakdown and pit nucleation. The PDM provides a deterministic description of passivity breakdown on metals and alloys [7, 15-20]

and hence provides a suitable basis for eventually predicting whether localized corrosion damage will occur in the operating repository. One of the purposes of the present study of passivity breakdown on copper is to assess the ability PDM for quantitatively describing passivity breakdown on copper in the presence of chloride ion and sulphide ion; conditions under which the barrier layer is unequivocally Cu_2S.

The influence of dissolved sulphide species on the electrochemical behaviour of copper and its alloys is complex and no completely satisfactory mechanism has yet been reported. Several studies of copper corrosion in sulphide-polluted environments have revealed that copper forms a bilayer corrosion product comprising an inner ("barrier") layer of Cu_2S and a thicker CuS outer layer [21-23]. Chialvo and Ariva [21] proposed that reaction of copper in alkaline sodium sulphide solutions undergoes the following path of sequential steps: Cu/electrolyte → Cu/$Cu_{1.8}S$/electrolyte → Cu/$Cu_{1.8}S$/Cu_2S/electrolyte → Cu/$Cu_{1.8}S$/Cu_2S/CuS/electrolyte; that is, they postulate the formation of a tri-layer passive film. They concluded that cuprous sulphide (Cu_2S) is predominantly formed at potentials lower than -0.6 V vs. SHE, while cupric sulphide (CuS) forms after long electrolysis at higher potentials. The work of Macdonald et al. [24] suggested the formation of a duplex sulphide film on Cu-Ni alloys in deaerated sea water containing sulphide species. Syrett [25], on the other hand, reported that the bilayer film comprises an oxide barrier (inner) layer and a Cu_2S (or $Cu_{2-x}S$) outer layer. This oxide/sulphide bilayer structure is likely to be seen in a repository only while significant oxygen is present in the environment; that is during the initial "oxic" period. Once the initially trapped oxygen has been consumed during this initial oxic period (a few decades), and the system becomes more reducing in nature (during the much longer anoxic period) the formation of an oxide barrier layer is judged on the basis of thermodynamics to be unlikely. Thus, based on the thermodynamic information of the system, Macdonald et al. [26] postulate that the presence of sulphide species in a sea water solution will shift the corrosion potential to more active values that could satisfy the thermodynamic criterion for spontaneous formation of cuprous sulphide with hydrogen evolution acting as the principal cathodic partial reaction.

The "activating" role of sulphide ion on the corrosion of copper is, perhaps, best illustrated by the Corrosion Domain Diagrams for copper in the absence [Fig. 1.2 (a)] and in the presence [Fig. 1.2 (b)] of sulphide. In these figures, as noted above, the quantity P is defined as $P = f_{H_2}^{1/2} a_{Cu^+}$ and $P = \frac{f_{H_2}}{a_{HS^-}}$, respectively, corresponding to the

corrosion reactions: $Cu + H^+ \rightarrow Cu^+ + 1/2H_2$ and $2Cu + HS^- + H^+ \rightarrow Cu_2S + H_2$. The quantity, P^e, corresponds to the value of the partial reaction quotient, P, at equilibrium. The diagrams plot P vs pH and are divided into two regions: for $P > P^e$, copper is thermodynamically immune and corrosion cannot occur, whereas if $P < P_e$ corrosion is spontaneous. Thus, if P is initially below the equilibrium line, in a closed system, corrosion will occur and corrosion products (Cu^+, H_2) will accumulate adjacent to the metal surface, resulting in an increase in the value of P. After a sufficiently long time, $P = P^e$ for the prevailing temperature and further corrosion becomes limited by the rate of mass transport of the corrosion products away from the copper interface. The principal role of bisulphide ion (and many other polysulphide species, e.g., HS_x^-) is that the value of P^e shifts by 20 orders of magnitude in the positive direction making the immune state impossible to achieve practically. CDDs were originally derived by one of the present authors [27] to resolve a controversy raging in Sweden over the report by Hultqvist, et.al. [4-6] that copper corrodes in deaerated pure water, as determined by the evolution of hydrogen, whereas copper had always been considered to be immune under these conditions and hence its classification as being a "semi-noble" metal. With reference to Figure 1.2 (a) any combination of hydrogen fugacity (pressure) and cuprous ion activity for which $P > P^e$ suffices to render the copper immune and likewise any combination of these variables for which $P < P^e$ suffices to render corrosion spontaneous. In the absence of exact values for the hydrogen fugacity (pressure) and cuprous ion activity in the experiments of Hultqvist et.al. [4-6] and those of their detractors, it is suggested that the relative values of P and P^e provide a thermodynamically-viable resolution of the controversy.

Recently, several studies on the corrosion and electrochemistry of copper in sulphide-containing granitic repository environments have been published [13, 28-33]. These studies were performed in sodium chloride solutions containing different concentrations of sulphide species that are expected to be present in the repository in Sweden. Chen et al. [28] studied the kinetics of the copper corrosion in a neutral sodium chloride solution containing a small concentration of sulphide ion as a function of time under open circuit potential conditions. Their results revealed that, while chloride ion can influence the morphology of the copper sulphide deposits, there is no evidence of its direct role in the copper dissolution reaction. Combined electrochemical and morphological studies in their work have shown that the corrosion film formed on the copper surface comprised a single layer of Cu_2S, with the thickness increasing with immersion time [28]. Mott-Schottky analysis by Ling et al. [34] indicate that a bi-layer sulphide film forms, comprising a p-type barrier layer of Cu_2S and probably an outer layer of CuS, which is n-

type in electronic character. The outer layer was not observed to form at 25°C and at 50°C, but was observed to form intermittently at 75°C. Given this, we replace, in the Point Defect Model (PDM), the usual oxide barrier layer of a metal-H_2O system with the metal sulphide (Cu_2S) in formulating of physico-electrochemical description of the passive state on copper in sulphide-containing, aqueous media.

The PDM [7, 8, 15-20] proposes that cation vacancies$\left(V_{\mathrm{M}}^{\chi'}\right)$, generated at the film/solution interface by ejection of a cation from the film, move to the metal/film interface, and are annihilated by cation injection into the film from the metal.

$$m + V_{\mathrm{M}}^{\chi'} \rightarrow M_{\mathrm{M}} + v_{\mathrm{m}} + \chi e' \tag{1.3}$$

where m and v_{m} are a metal atom and a metal vacancy in the metal phase, respectively; and $V_{\mathrm{M}}^{\chi'}$ and M_{M} are a cation vacancy and a cation in normal cation sites on the cation sub-lattice of the barrier layer. The annihilation rate of the cation vacancies $\left(V_{\mathrm{M}}^{\chi'}\right)$ at the metal/film interface due to Reaction (1.3) is designated as J_{m}. Aggressive anion absorption (e.g. chloride anion) into surface sulfur vacancies $(V_{\mathrm{S}}^{\cdot\cdot})$ is postulated to catalyze the generation of cation vacancies possibly via the Schottky pair reaction $\left[Null \leftrightarrow V_{\mathrm{M}}^{\chi'} + \frac{\chi}{2} V_{\mathrm{S}}^{\cdot\cdot}\right]$ or by anion-assisted, cation extraction (ion desorption/vacancy pair generation). Both processes are autocatalytic in the sulfur vacancy, in that the sulfur vacancies are regenerated at the periphery of the vacancy condensate and hence are available to absorb additional aggressive anion. The increased concentration of cation vacancies in the film at the film/solution (f/s) interface leads to an enhanced flux of the cation vacancies (J_{ca}) towards the metal/film (m/f) interface [7, 8, 15-20]. If the cation vacancies ($V_{\mathrm{M}}^{\chi'}$) cannot be totally annihilated at the m/f interface by Reaction (1.3), or if the vacancies on the metal lattice (v_{m}) on the metal side of the m/f interface cannot be annihilated by process such as dislocation climb or by diffusion into the bulk metal, the excess vacancies arriving at the m/f interface is given by ($J_{\mathrm{ca}} > J_{\mathrm{m}}$) and the excess vacancies must condense on the respective lattices. This process will continue until the areal vacancy concentration in the condensate exceeds a critical value (ξ), resulting in local separation of the barrier layer from the substrate metal. This local vacancy condensation/separation process continues at the periphery of the condensate causing the condensate to expand and preventing the film from penetrating into the substrate via the generation of sulfur vacancies via the reaction

$$m \rightarrow M_{\mathrm{M}} + \frac{\chi}{2} V_{\mathrm{S}}^{\cdot\cdot} + \chi e' \tag{1.4}$$

However, dissolution continues at the f/s interface, with the result that the barrier layer over the condensate thins at a rate that is determined by the dissolution rate and, at some point, the ‘‘cap’’ (remnants of the barrier layer) over the condensate ruptures to mark a passivity breakdown event [7, 8, 15-20]. The critical areal concentration (#/cm^2) of cation vacancies that must condense (ξ) for separation to occur between the barrier layer and the metal substrate is determined by the structures of the metal and the barrier layer, depending on whether condensation is envisioned to occur on the metal lattice or on the cation sub-lattice of the film. According to this mechanism, taking into account only chloride anion adsorption/Schottky-pair vacancy generation, the following relationship for the critical breakdown potential (V_c) was derived [7, 8, 14-16].

$$V_c = \frac{4.606RT}{\chi\alpha F}\log\left(\frac{b}{D}\right) - \frac{2.303RT}{\alpha F}\log(a_{\mathrm{Cl}^-}) \tag{1.5}$$

$$b = \frac{RTJ_m\Omega}{\chi F\varepsilon N_A} \times exp\left(\frac{\Delta G_S^0 + \frac{\chi}{2}\Delta G_A^0 - \frac{\chi}{2}\beta F\mathrm{pH} - \frac{\chi}{2}F\phi_{f/s}^0}{RT}\right) \tag{1.6}$$

$$\phi_{f/s} = \phi_{f/s}^0 + \alpha V + \beta\mathrm{pH} \tag{1.7}$$

where a_{Cl^-} is the chloride ion activity, D is the diffusivity of the cation vacancy in the barrier layer, and b is defined in Eq. (1.6). The parameters χ, ε, and Ω are the sulphide stoichiometry ($CuS_{\chi/2}$), the electric field strength within the barrier layer, and the volume per mole of the cations in the film. The electric field strength is postulated to be buffered by Esaki (band-to-band) tunneling and hence is independent of applied voltage. In this process, if any stress causes the electric field to increase (e.g., a sudden increase in the applied voltage), an internal tunneling current, which is a function of the tunneling distance between the valence and conduction bands at constant energy produces a separation of charge that opposes the field. The electric field strength within the barrier layer is in the expected range of 1-5×10^6 V/cm [7, 8] and is sweep rate-independent. The quantities ΔG_S^0 and ΔG_A^0 are the change in standard Gibbs energy for the Schottky-pair reaction and for the absorption of chloride anions into sulfur vacancies at the film/solution interface, respectively. The parameters α and β are the dependencies of the potential drop across the film/solution interface ($\phi_{f/s}$) on the applied potential V and pH, respectively. $\phi_{f/s}^0$ is the value of $\phi_{f/s}$ in the standard state of V= 0 and pH = 0. R is the gas constant, T is the Kelvin temperature, F is Faraday’s constant, and N_A is Avogadro’s number.

According to the PDM, passivity breakdown occurs at sites on the surface that are characterized by high cation vacancy diffusivity [8]. These sites are considered to include the regions of high local disorder

in the structure of the barrier layer that might exist, for example, at points of intersection of the barrier layer with inclusions (e.g., MnS in stainless steels [35]) and other precipitates (e.g., $Cr_{23}C_6$, also in stainless steels [36]). Cassaignon et.al. [37] revealed that the diffusivity of copper vacancies depends strongly on the composition and its value falls in the range of 1.0×10^{-6} $cm^2\cdot s^{-1}$ to 1.2×10^{-10} $cm^2\cdot s^{-1}$ at room temperature. It should be mentioned that all of the reported values in the literature were measured on either natural copper sulphide electrodes or on electrodes prepared by pressing copper sulphide powders into pellets. However, Macdonald et.al. [2] reported that the diffusivity of copper vacancies in the copper sulphide films that grown electrochemically is in the range of 10^{-11} $cm^2\cdot s^{-1}$ to 10^{-13} $cm^2\cdot s^{-1}$, depending on the temperature.

The potential breakdown sites are assumed to be distributed normally with respect to the cation vacancy diffusivity with the distribution being characterized by a mean value, $\overline{D}$, and a standard deviation, σ_D. Based on this postulate, an analytical distribution function for V_c is readily derived as Eq. (1.8) [18, 19]:

$$\frac{dN}{dV_c} = \frac{-\gamma' D}{\sqrt{2}\pi\cdot\sigma_D} exp\left[-\left(\frac{D-\overline{D}}{\sqrt{2}\sigma_D}\right)^2\right] = \frac{-b\gamma'}{\sqrt{2}\pi\cdot\sigma_D\cdot a_{Cl^-}^{\chi/2}} exp\left[\frac{-\left(e^{-\gamma' V_c}-e^{-\gamma'\overline{V_c}}\right)^2 b^2}{2\sigma_D^2 a_{Cl^-}^{\chi}}\right] \exp(-\gamma' V_c) \tag{1.8}$$

where $\gamma' = \frac{\chi\alpha F}{2RT}$, and $\overline{V_c}$ is the mean critical breakdown potential, which can be calculated as,

$$\overline{V_c} = \frac{1}{\gamma'} ln\left(\frac{b}{\overline{D}} \times a_{Cl^-}^{\chi/2}\right) \tag{1.9}$$

Importantly, V_c is predicted to follow a near-normal distribution, as has been observed experimentally [38]. The cumulative probability in the critical breakdown potential (V_c) is defined as Eq. (1.10), where $P(V_c)$ represents the percentage of breakdown sites at V_c of all possible breakdown sites that are activated[15, 16].

$$P(V_c) = 100 \times \frac{\int_{-\infty}^{V_c}\left(\frac{dN}{dV_c}\right)dV_c}{\int_{-\infty}^{+\infty}\left(\frac{dN}{dV_c}\right)dV_c} \tag{1.10}$$

The relationship of $P(V_c)$ versus V_c as given by Equations (1.8) to (1.10), in comparison with experiment, provides a sensitive test of the

fundamental nature of, and the theory for, the distribution of breakdown sites on the metal surface.

2.4. References

1. J. Chen, Z. Qin, and D. W. Shoesmith, "The key parameters determining the structure and properties of the sulphide films formed on Cu surfaces in anaerobic sulphide solutions", Paper 14, LTC2013, Asahikawa, Japan, Oct 6-10, 2013.
2. D. D. Macdonald, S. Sharifi-Asl, and G.R. Engelhardt, "Issues in the Corrosion of Copper in a Swedish High Level Nuclear Waste Repository: Phase III. Role of Sulphide Ion in Anodic and Cathodic Processes", Technical Note 2014:57, Swedish Radiation Safety Authority, Sweden (2014).
3. D. D. Macdonald, "Passivity: The Key to Our Metals-Based Civilization", Pure Appl. Chem., 71, 951 (1999).
4. G. Hultqvist, Hydrogen evolution in corrosion of copper in pure water, Corros. Sci., 26 (1986) 173-177.
5. G. Hultqvist, G. K. Chuah, and K. L. Tan, Comments on hydrogen evolution from the corrosion of pure copper, Corros. Sci., 29 (1989) 1371-1377.
6. P. Szakalos, G. Hultqvist, and G. Wikmark, Corrosion of copper by water, Electrochem. Solid-State Lett. 10 (2007) C63-C67.
7. D. D. Macdonald, The point defect model for the passive state, J. Electrochem. Soc., 139(12) (1992) 3434-3449.
8. D. D. Macdonald, Passivity: The key to our metals-based civilization, Pure Appl. Chem., 71 (1999) 951-986.
9. D. D. Macdonald and S. Sharifi-Asl, Is copper immune when in contact with water and aqueous solutions: Phase I, TR 2011: 09, SSM, Stockholm, Sweden (2011).
10. J. M. Smith, Z. Qin, F. King, L. Werme, and D. W. Shoesmith, The electrochemistry of copper in aqueous sulphide solutions, Scientific Basis for Nuclear Waste Management XXIX. Symposium (Materials Research Society Symposium Proceedings), 932 (2006) 869-75.
11. J. Chen, Z. Qin, and D. W. and Shoesmith, Rate controlling reactions for copper corrosion in anaerobic aqueous sulphide solutions, Corros. Eng. Sci. and Tech., 46(2) (2011) 138-141.
12. J. M. Smith, Z. Qin, D. W. Shoesmith, F. King, and L. Werme, Source: Corrosion of copper nuclear waste containers in aqueous sulphide solutions, Scientific Basis for Nuclear Waste Management XXVII (Materials Research Society Symposium Proceedings), 824 (2004) 45-50.
13. J. Chen, Z. Qin, and D. W. Shoesmith, Long-term corrosion of copper in a dilute anaerobic sulphide solution, Electrochim. Acta, 56(23) (2011) 7854-7861.

14. F. King, L. Ahonen, C. Taxén, U. Vuorinen, L. Werme, Copper corrosion under expected conditions in a deep geologic repository, Swedish Nuclear Fuel and Waste Management Co., Report, Technical Report, SKB TR-01-23 (2001).
15. D. D. Macdonald, M. Urquidi-Macdonald, Corrosion damage function - interface between corrosion science and engineering, CorrosIon, 48 (5) (1992) 354-367.
16. L. F. Lin, C. Y. Chao, D. D. Macdonald, A point-defect model for anodic passive films. 2. chemical breakdown and pit initiation, J. Electrochem. Soc., 128 (1981) 1194-1198.
17. C. Y. Chao, L. F. Lin, D. D. Macdonald, A point-defect model for anodic passive films. 1. film growth-kinetics, J. Electrochem. Soc., 128 (1981) 1187-1194.
18. D. D. Macdonald, M. Urquidi-Macdonald, Distribution-functions for the breakdown of passive films, Electrochim. Acta, 31(8) (1986) 1079-1086.
19. M. Urquidi-Macdonald, D. D. Macdonald, Theoretical distribution-functions for the breakdown of passive films, J. Electrochem. Soc., 134 (1987) 41-46.
20. M. Urquidi-Macdonald, D. D. Macdonald, Theoretical-analysis of the effects of alloying elements on distribution-functions of passivity breakdown, J. Electrochem. Soc., 136 (1989) 961-967.
21. M. G. De Chialvo and A. Arvia, The electrochemical behavior of copper in alkaline solutions containing sodium sulphide, J. Appl. Electrochem., 15 (1985) 685-696.
22. V. Moll, Corrosion and passivity of copper in solutions containing sodium sulphide. Analysis of potentiostatic current transients, Electrochim. Acta, 30 (1985) 1011-1016.
23. E. Khairy and N. Darwish, Studies on copper-semiconducting layer-electrolyte systems ii. Galvanostatic anodic polarization of $Cu/Cu_2S/S^{2-}$ applying stationary and rectangular pulse techniques, Corros. Sci., 13 (1973) 149-164.
24. D. D. Macdonald, B. C. Syrett, and S. S. Wing, Tech. Report, Off. Nav. Res. (1978).
25. B. Syrett, The mechanism of accelerated corrosion of copper-nickel alloys in sulphide-polluted seawater, Corros. Sci., 21 (1981) 187-209.
26. D. D. Macdonald, B. C. Syrett, and S. S. Wing, Corrosion of Cu-Ni alloys-706 and alloys-715 in flowing sea-water. 2. Effect of dissolved sulphide, Corrosion, 35 (1979) 367-378.
27. D. D. Macdonald., Is copper immune when in contact with water, in mechanisms of copper corrosion in aqueous environments, Report: Swedish National Council for Nuclear Waste's Scientific Workshop, Stockholm, Sweden (2009).

28. J. Chen, Z. Qin, and D. W. Shoesmith, Kinetics of corrosion film growth on copper in neutral chloride solutions containing small concentrations of sulphide, J. Electrochem. Soc., 157 (2010) C338-C345.
29. J. M. Smith, J. C. Wren, M. Odziemkowski, and D. W. Shoesmith, The Electrochemical Response of Preoxidized Copper in Aqueous Sulphide Solutions, J. Electrochem. Soc., 154 (2007) C431-C438.
30. J. M. Smith, Z. Qin, F. King, and D. W. Shoesmith, The Influence of Chloride on the Corrosion of Copper Waste Containers in Aqueous Sulphide Solutions, Workshop on Sulphur-Assisted Corrosion in Nuclear Disposal Systems (Brussels, Belgium, Oct. 21-23, 2008), edited by D. Fèron, et al., European Federation of Corrosion Series 59 (2008) 109-123.
31. J. M. Smith, Z. Qin, and D. Shoesmith, Electrochemical Impedance Studies of the Growth of Sulphide Films on Copper, 17th Proc. Int. Corros. Cong., (2009) 1-9.
32. I. Betova et al., Corrosion of Copper in Simulated Nuclear Waste Repository Conditions, Electrochem. Solid-State Lett., 6 (2003) B19-B22.
33. M. Bojinov and T. Laitinen, MRS . Res. Soc. Symp. Proc., 807 (2004) 1-6.
34. Y. Ling, M. L. Taylor, Sharifiasl S, et al. The Semiconducting Properties and Impedance Analysis of Passive Films on Copper in Anoxic Sulphide-Containing Solutions from the Viewpoint of the Point Defect Model, ECS Transactions, 50(31) (2013)53-67.
35. D. D. Macdonald, D.F. Heaney, Effect of variable intensity ultraviolet radiation on passivity breakdown of AISI Type 304 stainless steel, Corros. Sci., 42 (2000) 1779-1799.
36. Z. Szklarska-Smialowska, Pitting Corrosion of Metals, NACE, Houston, Texas, 1986.
37. S. Cassaignon, T. Pauporté, J. F. Guillemoles, and J. Vedel, Ionics, 4 (1998) 364-371.
38. T. Shibata, T. Takeyama, Stochastic Theory of Pitting Corrosion, Corrosion, 33 (7) (1977) 243-251.

3. Research Objectives

The objectives of this research are the measurement of the distribution in the breakdown potential that will be used eventually to estimate the propensity toward pitting potential of the copper canister at different chloride concentrations, solution pH values, and temperature in the repository over the corrosion evolutionary path (CEP). The Phase IV work follows on that accomplished in Phases I, II, and III, in order to provide a better and more accurate definition of the localized corrosion processes and to estimate important parameter values for modeling the development of localized corrosion damage on pure copper surface. Using more advanced damage function analysis (DFA) [1-7], which is not reported in the present study, the work will eventually yield the development of localized corrosion damage that is expected to develop as the repository evolves over the planned storage period of 100,000 to 1,000,000 years. The measurements reported from the Phase IV work include the following.

3.1. Task 1: Measurement of the Passivity Breakdown Potential under Different Environmental Conditions

To determine passivity breakdown potentials, potentiodynamic polarization was applied by sweeping potential in the positive direction at a certain potential scan rate until breakdown was observed. Polarization was continued until the current density suddenly increased to over 10^{-4}A/cm^2. The breakdown potential was then measured as a function of temperature, chloride concentration, and pH. Also, the breakdown potential was measured potentiodynamically at different potential scan rates, in order to ascertain the relationship between the breakdown potential and potential scan rate, which in turn is a definitive test of the PDM [5-9]. Moreover, the statistical distribution of breakdown potential was obtained by potentiodynamic polarization at a scan rate of 0.1667 mV/s in typically twenty replicate experiments.

3.2. Task 2: Extract Parameter Values for the Distribution Function

Experimental relationships between the breakdown potential (V_c) and the chloride activity, pH, and potential scan rate yield important parameters values for the PDM. The dependencies of the potential drop across the film/solution interface (f/s) on the applied potential

and pH, α and β, respectively, can be computed from the linear relationship between V_c and chloride activity and pH. Moreover, by analyzing V_c vs. $v^{1/2}$ correlations, the critical cation vacancy concentration (ξ) leading to passivity breakdown on copper could be determined from the PDM. Meanwhile, other parameters for the distribution function are obtained from optimization of the PDM on electrochemical impedance spectroscopy data, as reported in Phase III [10].

3.3. Task 3: Prediction of the Cumulative Probabilities in the Breakdown Potential

It is possible to quantitatively predict the breakdown potential and its distribution under any given chloride concentration at any temperature and pH after we determine the parameters values of the distribution function parameters in the PDM, in addition to the other constants. As an evaluation for this quantitative prediction, the breakdown potential and its distribution for copper in simulated sulphide- and chloride-containing granitic rock ground water are calculated, and are then compared with some measured breakdown potential distributions. This will assess the ability of the PDM to account for passivity breakdown and provide important parameter values for more accurately modeling the development of localized corrosion damage on copper under the repository condition.

3.4. References

1. D.D. Macdonald, G.R. Engelhardt, Predictive modeling of corrosion, in: J.A. Richardson, R.A. Cottis, R. Lindsay, S. Lyon, J.D. Scantlebury, H. Stott, M. Graham (Eds.), Shreir's Corrosion, vol. 2, Elsevier, Amsterdam, 2010, p. 1630.
2. G. Engelhardt, D.D. Macdonald, Y. Zhang, B. Dooley, Deterministic prediction of corrosion damage in low pressure steam turbines, Power Plant Chem., 6 (11)(2004) 647.
3. D.D. Macdonald, C. Liu, M. Urquidi-Macdonald, G.H. Stickford, B. Hindin, A.K.Agrawal, K. Krist, Prediction And Measurement Of Fitting Damage Functions for Condensing Heat-Exchangers, Corrosion, 50 (10) (1994) 761.
4. G. Engelhardt, D.D. Macdonald, Deterministic prediction of pit depth distribution, Corrosion, 54 (6) (1998) 469.
5. M. Urquidi-Macdonald, D.D. Macdonald, Theoretical Distribution-Functions for the Breakdown Of Passive Films, J. Electrochem. Soc., 134 (1987) 41.

6. D.D. Macdonald, M. Urquidi-Macdonald, Corrosion Damage Function - Interface Between Corrosion Science And Engineering,. Corrosion, 48 (1992) 354.
7. D.D. Macdonald, Passivity - the key to our metals-based civilization, Pure Appl. Chem., 71 (1999) 951.
8. D.D. Macdonald, M. Urquidi-Macdonald, Distribution-Functions for the Breakdown Of Passive Films, Electrochim. Acta, 31 (8) (1986) 1079.
9. M. Urquidi-Macdonald, D.D. Macdonald, Theoretical-Analysis Of the Effects Of Alloying Elements on Distribution-Functions Of Passivity Breakdown, J. Electrochem. Soc., 136 (1989) 961.
10. D. D. Macdonald, S. Sharifi-Asl, and G.R. Engelhardt, Issues in the Corrosion of Copper in a Swedish High Level Nuclear Waste Repository: Phase III. Role of Sulphide Ion in Anodic and Cathodic Processes, Technical Note 2014:57, Swedish Radiation Safety Authority, Sweden (2014).

4. Passivity Breakdown on Copper: Influence of Chloride Ion

4.1. Introduction

As noted above, the initial event in the development of localized corrosion is passivity breakdown, followed by pit nucleation, growth, and repassivation. Because of this sequence, it is critically important to understand the mechanisms of the passivity breakdown and pit nucleation processes, especially when the alloy is exposed simultaneously to both corrosive species (i.e., HS^- and Cl^-). It is noted that chloride concentration (or activity) is an important environmental variable that has a great effect on the pitting potential and its distribution. This is because increasing chloride concentration decreases the mean breakdown potential (V_c), and also tends to decrease the standard deviation (σ_D) in the cation vacancy diffusivity (D). Contrariwise, when the chloride concentration decreases, the mean breakdown potential (V_c) and the standard deviation (σ_D) both increase. Not surprisingly, over the past 30 years, there have been many studies related to measuring the critical breakdown potential (V_c) of metals passivated with oxide barrier layers [1-3]; however, few studies have focused on the breakdown of copper sulphide films. Several theories have been developed to explain passivity breakdown and pit nucleation in stainless steels [1-7], but only the Point Defect Model (PDM) has achieved successful explanations of several commonly observed relationships and phenomena [4, 8], such as the linear dependence of the critical breakdown potential on $\log[Cl^-]$ with a slope that is greater than 2.303RT/F [9]; the dependence of the induction time on potential and $[Cl^-]$ [4]; the dependence of V_c on potential scan rate and the estimation of the concentration of cation vacancies in the cation vacancy condensate at the metal/film interface, which is postulated to be the precursor to passivity breakdown [10]; the distributions in V_c and t_{ind} [11]; photo-inhibition of passivity breakdown [12,13]; and the inhibition of pitting by minor alloying elements (e.g., Mo, W) in the substrate [14]. Here, we use the PDM to explore the critical breakdown potential of pure copper in the presence of sulphide and chloride ions.

4.2. Experimental

The electrochemical measurements were performed in a conventional three-electrode cell at ambient temperature (22±2 °C), using a working electrode (WE) made from pure copper rod (99.999%, Alfa

Aesar). A saturated calomel electrode (SCE) and a Pt plate were employed as reference electrode (RE) and counter electrode (CE), respectively. The reference electrode was connected to the cell through an electrolyte bridge/Luggin capillary.

The working electrode was mounted in epoxy resin with a 0.317 cm^2 area exposed to solution. The WE surface was abraded to a mirror finish with 600, 800 and 1200 SiC paper and finally polished using 0.1μm diamond polishing suspension. After polishing, the electrode was rinsed with deionized water (18.3 $M\Omega \cdot cm^{-1}$) and blow-dried with nitrogen gas. The electrolyte was 2×10^{-4} M sodium sulphide solution with different concentration of sodium chloride and different pH values (Table 3.1). The solutions with pH at 8 and 9 were established with 0.2 M borate buffer solution. A chloride concentration equal to 1M was selected for the pH-dependence study.

Table 3.1. Composition, measured pH of solutions

No.	Composition	Measured pH
1	0.01M NaCl+2x10^{-4}M Na_2S	9.21
2	0.05M NaCl+2x10^{-4}M Na_2S	9.19
3	0.1M NaCl+2x10^{-4}M Na_2S	9.15
4	0.5M NaCl+2x10^{-4}M Na_2S	9.07
5	1M NaCl+2x10^{-4}M Na_2S	8.93
6	5M NaCl+2x10^{-4}M Na_2S	8.91
7	1M NaCl+2x10^{-4}M Na_2S+0.2M borate buffer	8.00
8	1M NaCl+2x10^{-4}M Na_2S+0.2M borate buffer	10.01

The electrolyte was deaerated prior to an experiment with high purity nitrogen (HP, 99.99%) for approximately two hours and a stable flow of nitrogen was maintained during the experiment itself. The WE was initially reduced potentiostatically at -1.2 V vs. SCE for 20 min to remove any air-formed oxide on the surface. A two-hour rest at the open circuit potential (OCP) was then allowed before potentiodynamic polarization (PD) was commenced (scan rate = 0.1667mV/second). The potentiodynamic experiments were typically repeated 20 times to obtain a statistical distribution of the critical breakdown potential (V_c). All electrochemical experiments were performed using a Solartron 1280B Electrochemical Measurement System and the data were collected using CorrWare/CorrView.

Figure 3.1 A photograph of the cell used in the experiments.

4.3. Results and discussion

Typical potentiodynamic polarization curves for copper in deaerated sodium sulphide solutions (pH = 9 ± 0.2) as a function of chloride concentration are shown in Figure 3.2. The polarization curves are characterized by flat passive regions followed by a rise in the current density at a potential that depends on the chloride concentration, due to passivity breakdown. The critical breakdown potentials are determined by the intersection of the tangent lines of current density in the passive range and for the post-passivity breakdown stage. It is evident that chloride plays an important role in passivity breakdown on copper, because as its concentration increases, the breakdown potential decreases by about -0.32V from V_c= -0.08V_{SCE} at [Cl^-] = 0.01 M to around V_c=-0.4V_{SCE} at [Cl^-] = 5M; a change similar to that observed for passivity breakdown on iron- and nickel-based alloys [8].

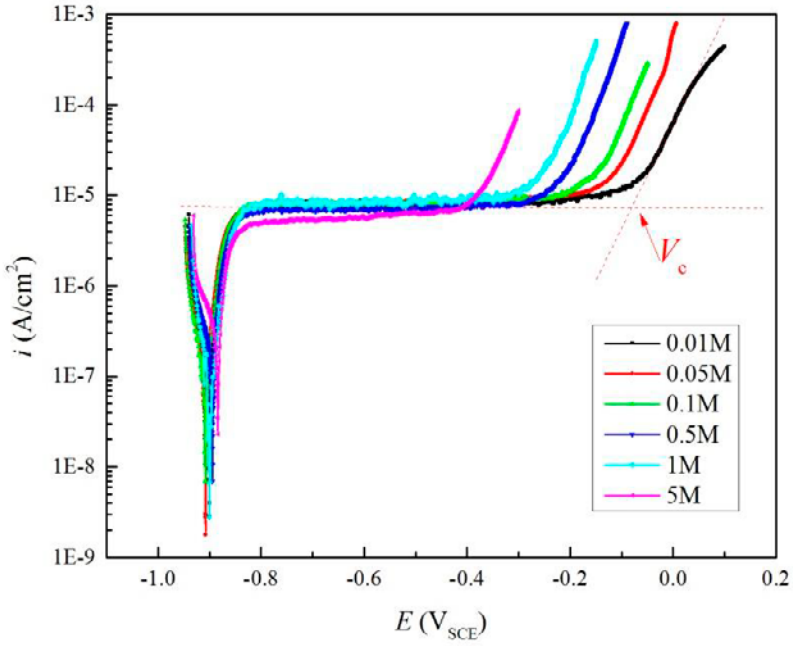

Figure 3.2. Typical potentiodynamic polarization curves for copper in deaerated 2×10^{-4}M Na_2S solutions (pH = 9±0.2) as a function of chloride concentration, indicating the determination of the critical breakdown potential (V_c).

The replicate potentiodynamic polarization curves and cumulative distributions for different solutions are presented in Figure 3.3 - 3.18. Parenthetically, it is noted that the critical breakdown potential measurements, as obtained in this study, demonstrate good reproducibility. The distributions are typically about 30mV in width. Compared with the good reproducibility of V_c, the passive current densities are more scattered, which might be the result of different surface microstructures on different samples.

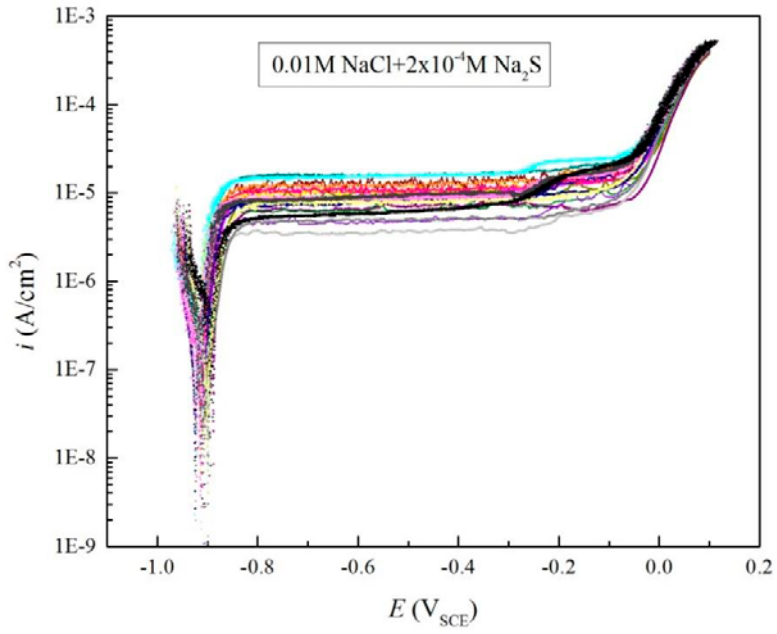

Figure 3.3. Replication (20 times) of the potentiodynamic polarization curves for copper in 0.01M NaCl + 2×10^{-4}M $Na_2S\cdot9H_2O$ solution.

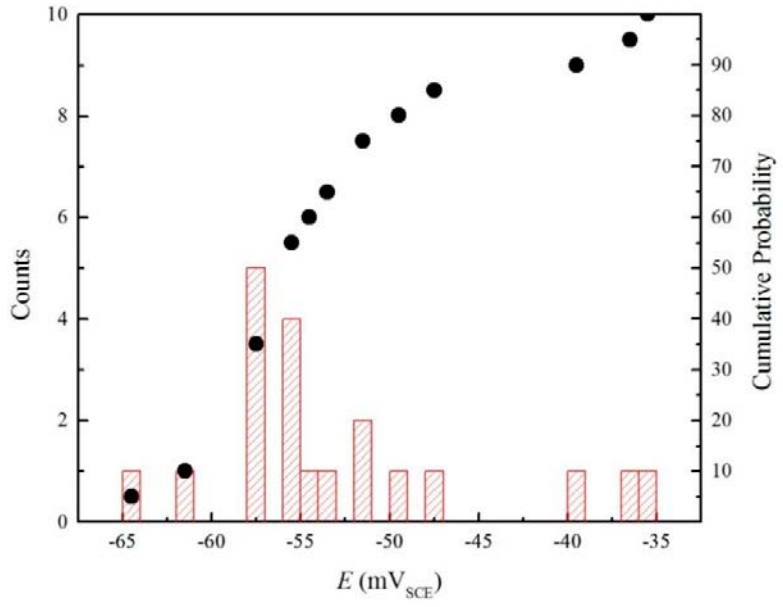

Figure 3.4. The statistics plot of V_c in 0.01M NaCl + 2×10^{-4}M $Na_2S\cdot9H_2O$ solutions. The bars represent the "counts" (number of samples exhibiting breakdown within a 1 mV region) and the closed points represent the cumulative probability.

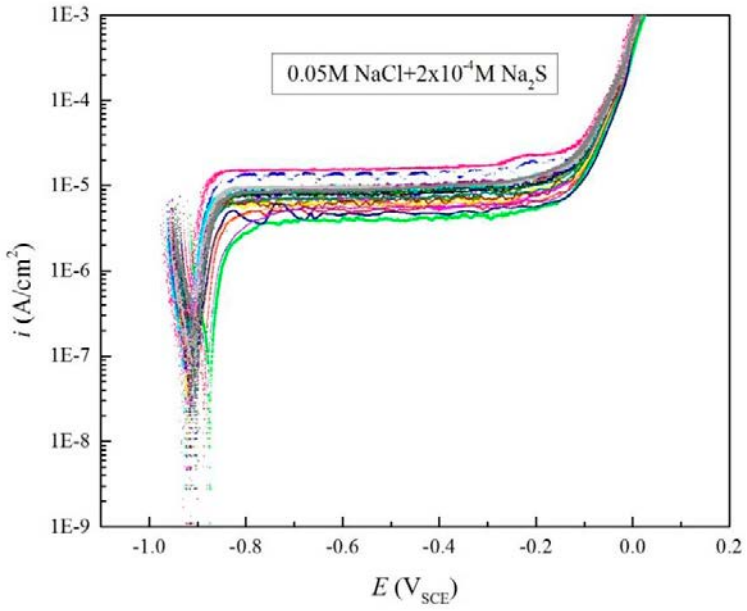

Figure 3.5. Replication (20 times) of the potentiodynamic polarization curves for copper in 0.05M NaCl + 2×10^{-4}M $Na_2S\cdot9H_2O$ solution.

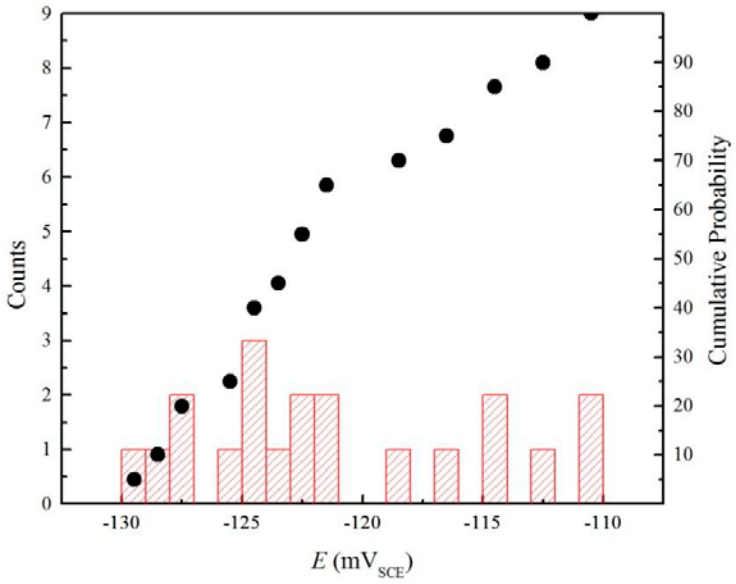

Figure 3.6. The statistics plot of V_c in 0.05M NaCl + 2×10^{-4}M $Na_2S\cdot9H_2O$ solutions. The bars represent the "counts" (number of samples exhibiting breakdown within a 1 mV region) and the closed points represent the cumulative probability.

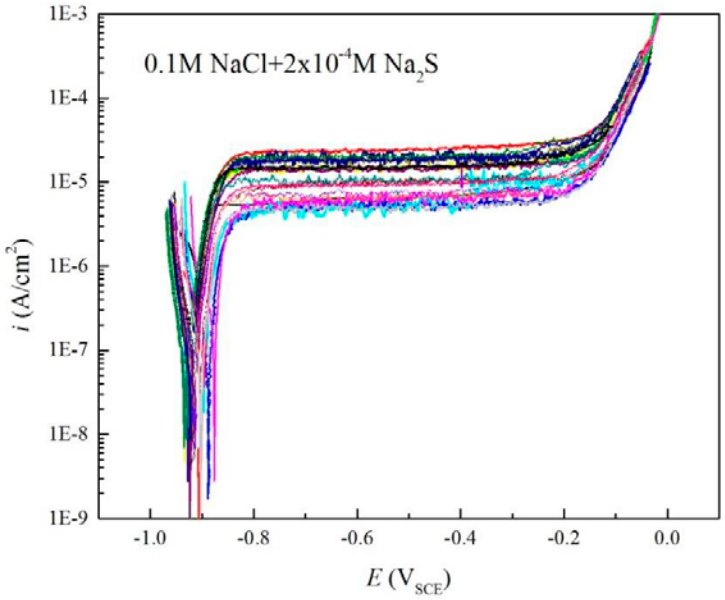

Figure 3.7. Replication (20 times) of the potentiodynamic polarization curves for copper in 0.1M NaCl + 2×10^{-4}M $Na_2S\cdot9H_2O$ solution.

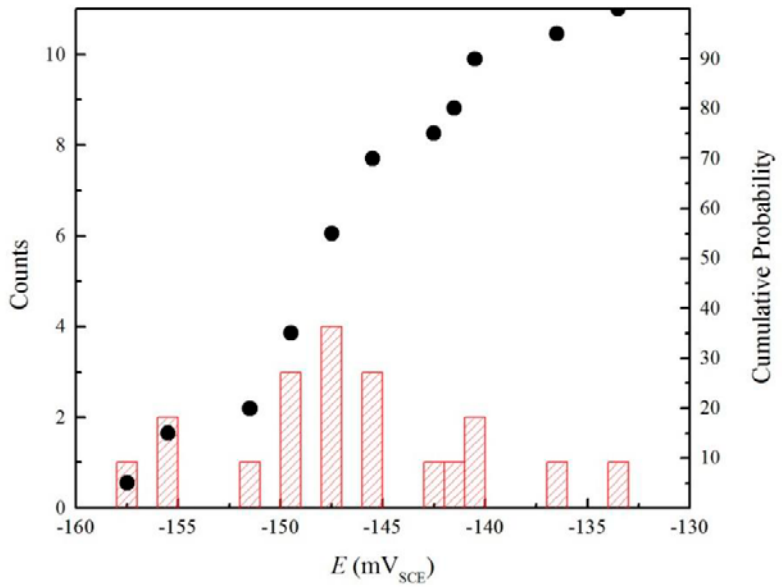

Figure 3.8. The statistics plot of V_c in 0.1M NaCl + 2×10^{-4}M $Na_2S\cdot9H_2O$ solutions. The bars represent the "counts" (number of samples exhibiting breakdown within a 1 mV region) and the closed points represent the cumulative probability.

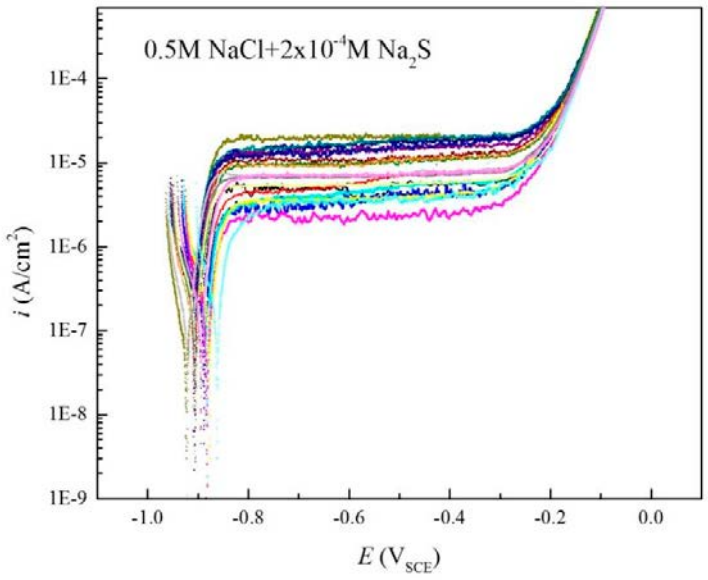

Figure 3.9. Replication (20 times) of the potentiodynamic polarization curves for copper in 0.5M NaCl + 2×10^{-4}M $Na_2S\cdot9H_2O$ solution.

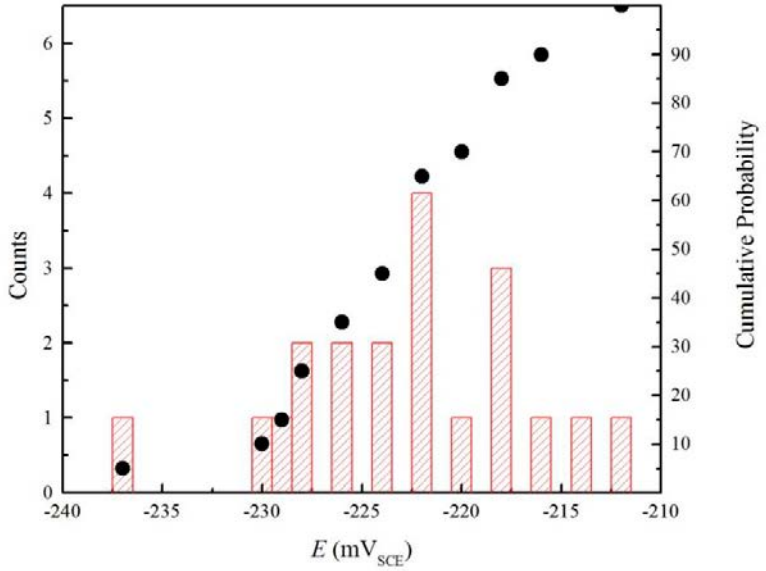

Figure 3.10. The statistics plot of V_c in 0.5M NaCl + 2×10^{-4}M $Na_2S\cdot9H_2O$ solutions. The bars represent the "counts" (number of samples exhibiting breakdown within a 1 mV region) and the closed points represent the cumulative probability.

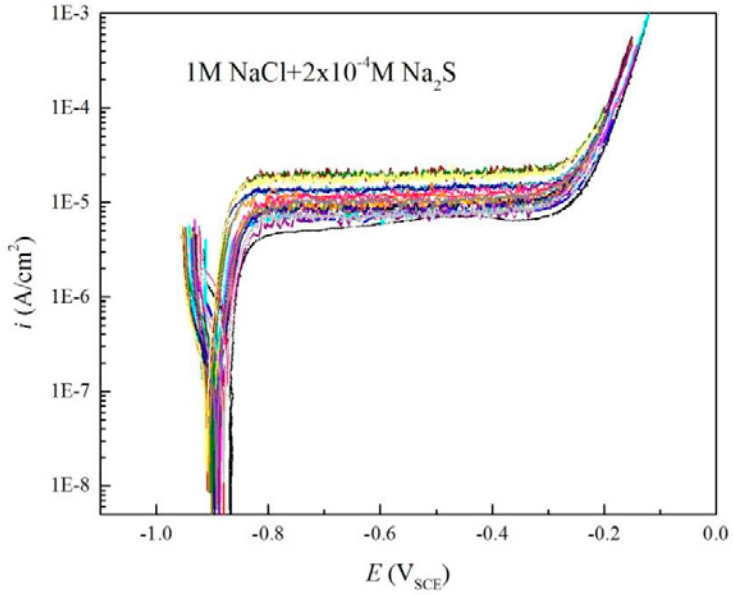

Figure 3.11. Replication (20 times) of the potentiodynamic polarization curves for copper in 1.0M NaCl + 2×10^{-4}M $Na_2S\cdot9H_2O$ solution.

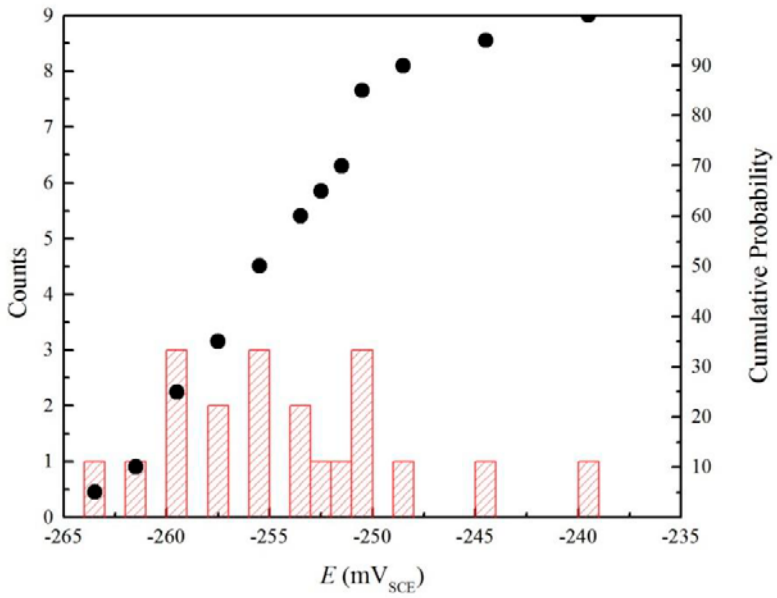

Figure 3.12. The statistics plot of V_c in 1.0M NaCl + 2×10^{-4}M $Na_2S\cdot9H_2O$ solutions. The bars represent the "counts" (number of samples exhibiting breakdown within a 1 mV region) and the closed points represent the cumulative probability.

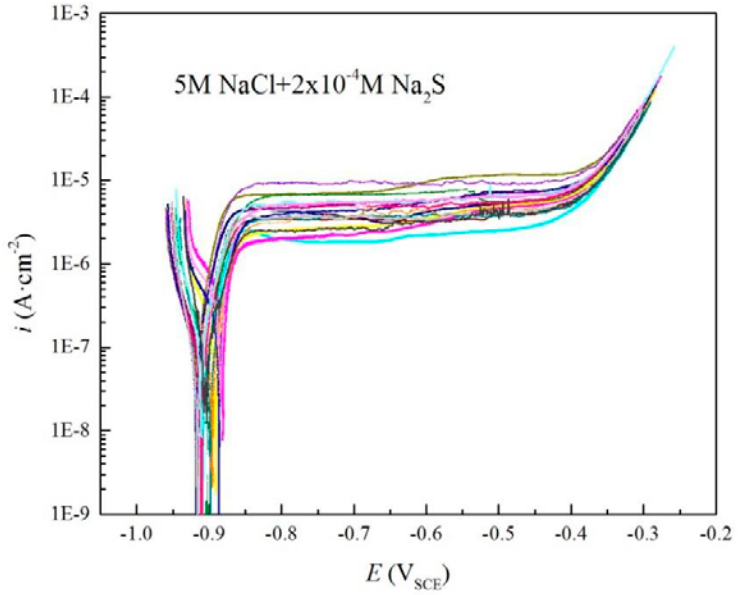

Figure 3.13. Replication (20 times) of the potentiodynamic polarization curves for copper in 5.0M NaCl + 2×10^{-4}M $Na_2S\cdot9H_2O$ solution.

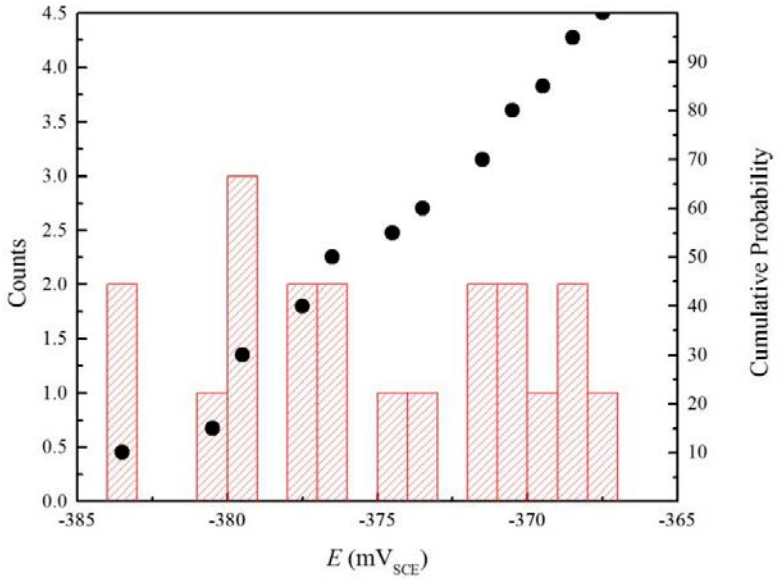

Figure 3.14. The statistics plot of V_c in 5.0M NaCl + 2×10^{-4}M $Na_2S\cdot9H_2O$ solutions. The bars represent the "counts" (number of samples exhibiting breakdown within a 1 mV region) and the closed points represent the cumulative probability.

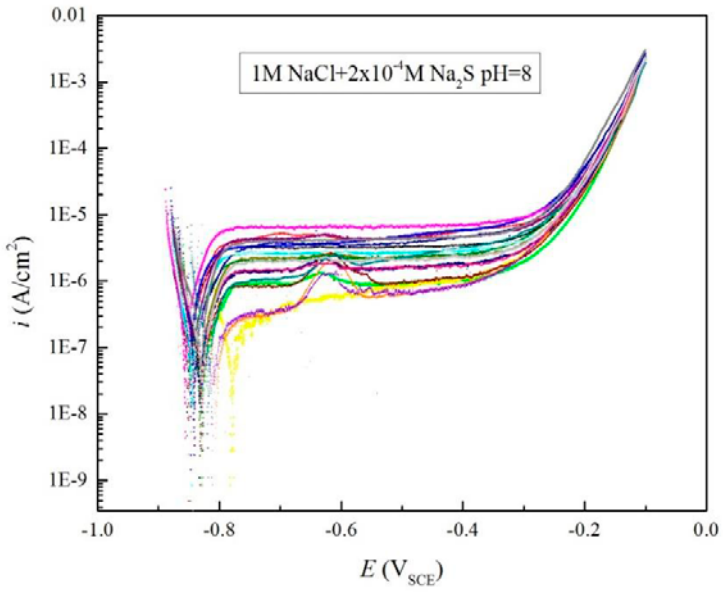

Figure 3.15. Replication (20 times) of the potentiodynamic polarization curves for copper in 1M NaCl + 2×10^{-4}M $Na_2S\cdot9H_2O$borate buffer solution (pH = 8).

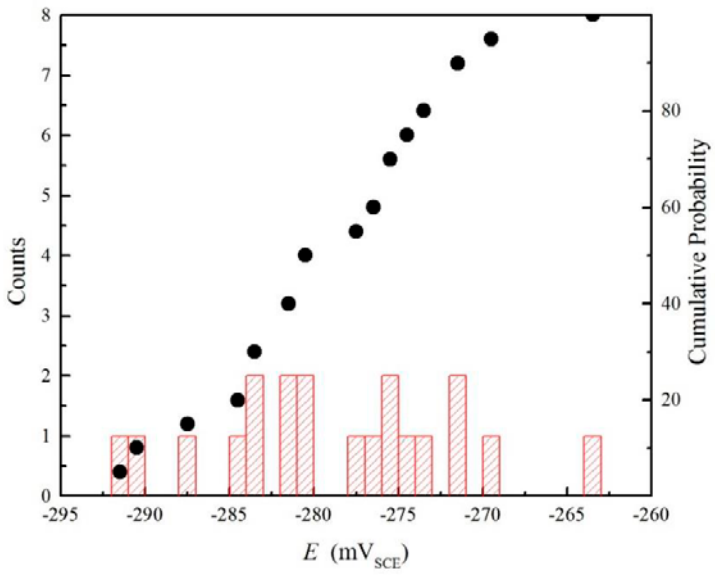

Figure 3.16. The statistics plot of V_c in 1.0M NaCl + 2×10^{-4}M $Na_2S\cdot9H_2O$ borate buffer solutions (pH = 8). The bars represent the "counts" (number of samples exhibiting breakdown within a 1 mV region) and the closed points represent the cumulative probability.

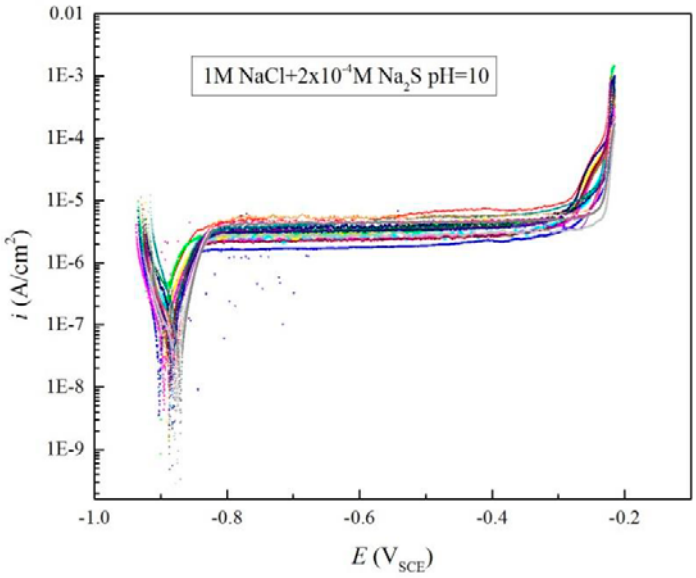

Figure 3.17. Replication (20 times) of the potentiodynamic polarization curves for copper in 1M NaCl + 2×10^{-4}M $Na_2S\cdot9H_2O$ borate buffer solution (pH = 10).

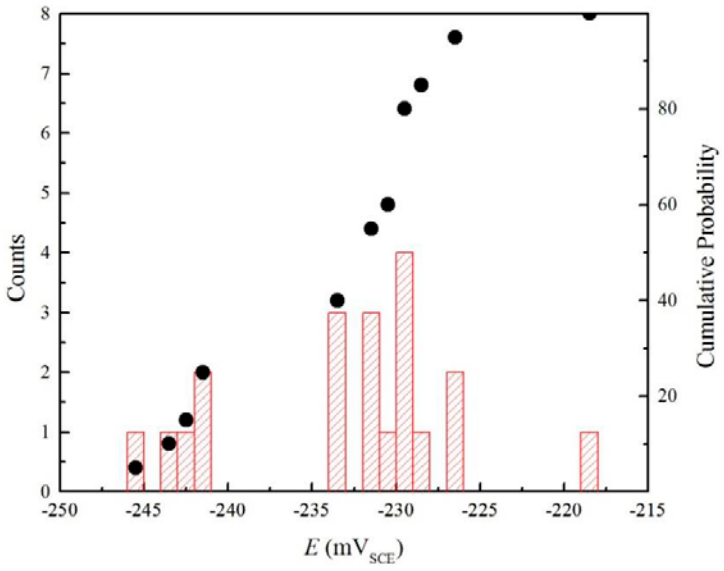

Figure 3.18. The statistics plot of V_c in 1.0M NaCl + 2×10^{-4}M $Na_2S\cdot9H_2O$ borate buffer solutions (pH =10). The bars represent the "counts" (number of samples exhibiting breakdown within a 1 mV region) and the closed points represent the cumulative probability.

In these plots, a normal distribution would be indicated by a straight line. Clearly, the plots deviate from being linear and this is the reason why they are termed "near-normal" in keeping with the theory [11].

As noted previously, the critical breakdown potential can be rewritten as Eq. (3.1) [4,8]:

$$V_c = V_0 - \frac{\beta}{\alpha}\mathrm{pH} - \frac{2.303RT}{\alpha F}\log[a_{\mathrm{Cl}^-}] \qquad (3.1)$$

where α is the polarizability of the film/solution interface and β is the dependence of the potential drop across the barrier layer/solution interface on pH; both can be determined by measuring V_c as a function of chloride concentration and pH. The mean in the distribution of critical breakdown potentials are -0.053 V_{SCE}, -0.121 V_{SCE}, -0.147 V_{SCE}, -0.223 V_{SCE}, -0.254 V_{SCE} and -0.375 V_{SCE} for chloride concentrations of 0.01, 0.05, 0.1, 0.5, 1.0 and 5.0 M, respectively, at pH = 9. The mean critical breakdown potential are -0.233 V_{SCE}, -0.254 V_{SCE} and -0.379 V_{SCE} for pH values of 8.00, 8.93, and 10.01, respectively, in 1.0 M chloride. Thus, Figure 3.19 shows the mean critical breakdown potential versus chloride ion activity correlation, with the mean molar activity coefficient ($\gamma_{\pm}$) for Cl^- in binary NaCl solutions of different concentrations [15, 16] being used to estimate the activity, a_{Cl^-}, of chloride ion in the buffer solutions. Figure 3.20 displays the mean V_c at different pH values for a chloride concentration of 1.0M. According to these data, V_c as a function of $[Cl^-]$ and pH can be described by the following equations:

$$V_c = -0.29023 - 0.12327\log[a_{\mathrm{Cl}^-}] \qquad (3.2)$$

and

$$V_c = -0.4618 + 0.0229\mathrm{pH} \qquad (3.3)$$

Based on Eqs.(3.2) and (3.3), α is determined to be 0.4751 and β is calculated to be -0.0109V. The V_0 values [Eq. (3.2)] are calculated to be -0.496 V_{SCE} and -0.484 V_{SCE} from Eqs. (3.2) and (3.3), respectively. The excellent agreement of the values for V_0 determined from the two sources demonstrates the viability of the PDM for describing passivity breakdown on copper in chloride-containing solutions.

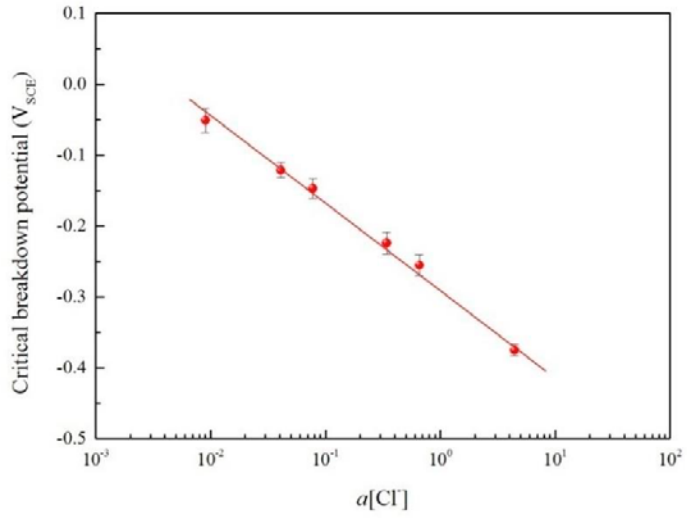

Figure 3.19. The mean in distribution in the critical breakdown potential as a function of chloride ion activity.

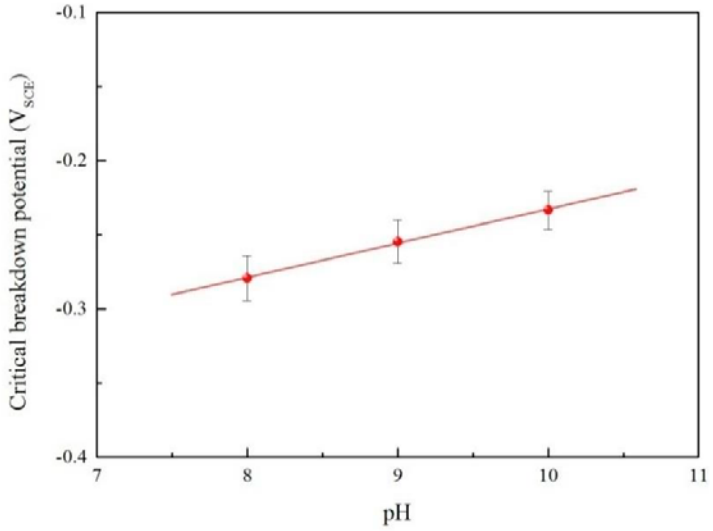

Figure 3.20. The mean in distribution in the critical breakdown potential for Cu in 1.0M NaCl + 2×10^{-4}M $Na_2S\cdot9H_2O$ solutions as a function of pH.

Under potentiodynamic polarization conditions, the breakdown potential (V_c) has been found previously to increase linearly with the square root of potential sweep rate ($v^{1/2}$) by Haruna and Macdonald [10] for nickel, Fonseca et. al. [17] for aluminum, Zhang [18] for Type 403SS, and by Zhang, Urquidi-Macdonald, and Macdonald [19] for the same alloy, among others [20], and is predicted by the Point Defect Model as Eq. (3.4) [10]. The PDM predicts that the gradient of V_c versus $v^{1/2}$ is essentially independent of the concentration of the aggressive species (chloride ion) and this was observed by Haruna and

Macdonald [10] and Zhang and Macdonald [19]. Due to the intrinsic uncertainty in the measured V_c (±15mV), and noting that the breakdown voltage is a distributed parameter reflecting an underlying distribution in the breakdown sites with regard to the cation vacancy diffusivity, [8, 21, 22], it is probably justified to use the measured V_c at a finite voltage sweep rate of, say, 0.1667 mV/s, as a practical way of minimizing the number of experiments that must be performed. In any event, the measured breakdown voltage may be corrected to zero scan rate by using the equation:

$$V_c(v) = \left(\frac{2\xi RT}{\chi\alpha F J_m}\right)^{1/2} v^{1/2} + V_c(v=0) \tag{3.4}$$

where $V_c(v=0)$ is defined as the breakdown potential at zero potential scan rate. Employing the value of α determined earlier and the ratio of (ξ/J_m) [15, 16], as determined from the slope (the value is 1.37 from Figure 3.21), if J_m is estimated from the passive current density immediately before passivity breakdown, the value of ξ, which is the critical areal (two-dimensional) concentration of condensed vacancies at the metal/barrier layer interface, can be determined. The quantity J_m, which is the rate of annihilation of cation vacancies at the metal/barrier layer interface at the breakdown potential, should be, at most, the value of the flux of cation vacancies (J_{ca}) moving through the barrier layer of the passive film from the barrier layer/solution interface to the metal/barrier layer interface. Moreover, for a p-type barrier layer, in which cation vacancies are the predominant conducting defects, J_{ca} may be calculated from the measured passive current at the point of breakdown (I_{ss}^{bd}) as

$$J_{ca} \leq \frac{I_{ss}^{bd} N_A}{\chi F} \tag{3.5}$$

where N_A is Avogadro's number and $\chi = 1$, for a passive film that comprises defective Cu_2S. The value of I_{ss}^{bd} was found to be approximately $10\mu A/cm^2$; and thus J_{ca} and J_m are estimated to be less than 6.24×10^{13} $cm^{-2}s^{-1}$. However, the value of I_{ss}^{bd} is measured potentiodynamically and the steady-state value is expected to be significantly smaller. It is for this reason that the inequality sign is included in Eq. (3.5). The value of the areal (two-dimensional) concentration of condensed cation vacancies, ξ, is therefore less than $1.09\times10^{15}cm^{-2}$. Because the concentrations of cations in the sulphide and of metal atoms in the alloy are related to the structures of Cu_2S and the substrate copper, respectively, we can estimate the values of ξ for vacancy condensation on the cation sublattice of the barrier layer on the film side of the interface or on the metal lattice on the substrate side of the boundary. Based on the available structural information, the areal atomic density for Cu and Cu_2S is 1.53×10^{15} cm^{-2} and 7.66×10^{14} cm^{-2}, respectively, indicating that, perhaps, vacancy

condensation occurs on the lattice of the copper substrate, although the data are probably not sufficiently accurate to make an unequivocal choice. Nevertheless, the agreement between theory and experiment provides powerful confirmation of the validity of the PDM for describing passivity breakdown on copper in sulphide-containing aqueous media.

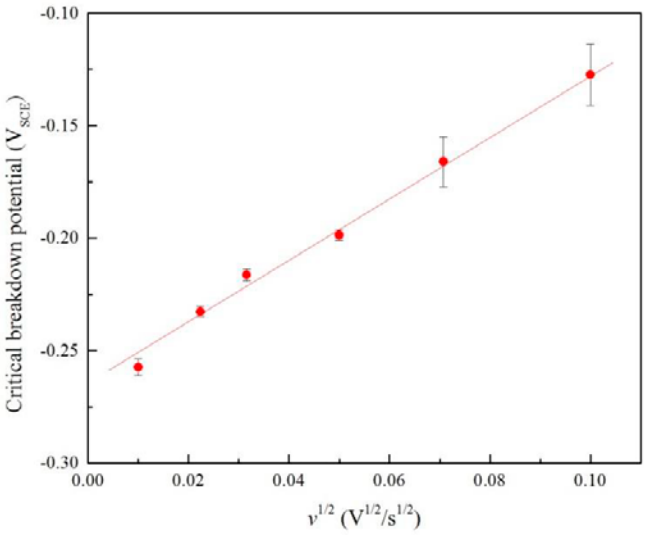

Figure 3.21. The measured breakdown potentials (V_c) at different potential scan rates (v) for Cu in 1.0M NaCl + 2×10^{-4}M $Na_2S\cdot9H_2O$ solutions.

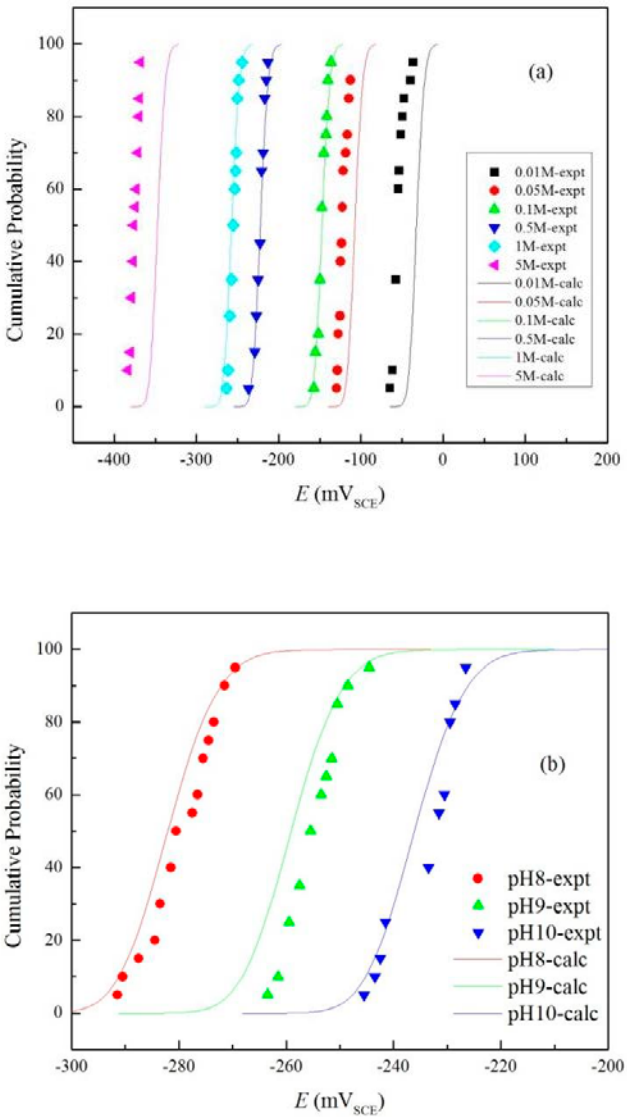

Figure 3.22. Calculated cumulative probabilities in the breakdown potential for Cu in deaerated sodium sulphide solution (pH = 9 ± 0.2) with different chloride concentrations (a) in 1.0M NaCl + 2×10^{-4}M $Na_2S\cdot9H_2O$ solutions and with different pH values (b), compared with the experimentally-determined distributions.

By using Eqs. (3.2)-(3.5), and the parameter values extracted from the above experiments (Table 3.2), the statistical cumulative probability distributions (CPDs) in the breakdown potential for copper in deaerated sodium sulphide solution containing different concentrations of chloride ion (pH = 9 ± 0.2) and in 1.0M NaCl + 2×10^{-4}M $Na_2S\cdot9H_2O$ solutions with different pH can be calculated. The calculated distributions using $\sigma_D = 0.07\overline{D}$ are plotted in Figure 3.22 as cumulative probabilities in the breakdown potential, and are compared with the experimental distributions in the breakdown

potential obtained from the potentiodynamic experiments performed in this study. Typically, these experiments were repeated 20 times, in order to obtain statistically valid distributions. The marked points are experimental data while the solid lines correspond to the calculated distributions. When the chloride concentration is in the range of 0.01M to 5M, the experimental distributions are narrow, and are in good agreement with the calculated distribution functions with a small $\sigma_{\mathrm{D}} = 0.07\overline{D}$. In any event, the experimental distributions in the breakdown potential are in satisfactory agreement with those calculated from the PDM with $\sigma_{\mathrm{D}} = 0.07\overline{D}$.

Table 3.2. Parameter values used in calculating cumulative probabilities in the critical breakdown potential for copper in deaerated sodium sulphide solution (pH = 9 ± 0.2) with different chloride concentrations at ambient temperature.

Parameter	**Value**	**Units**	**Source**
T, the absolute temperature	295.15	K	Defined
χ, the oxidation state of cation in barrier layer (Cu_2S)	1	Elementary charge	Defined
Ω, the molar volume of Cu_2S per cation	14.21	cm^3/mol	Defined
ε, the electric field strength	5×10^6	V/cm	Ref. 25
J_m, the rate of annihilation of cation vacancies at the metal/film interface	$\leq 6.24\times10^{13}$	No./(cm^2s)	Calculated
ξ, the critical areal cation vacancy concentration	1.09×10^{15}	No./cm^2	From Fig. 3.21
$\overline{D}$, the mean cation vacancy diffusion coefficient	4.22×10^{-13}	cm^2/s	Ref. 25
σ_D, the standard deviation for the cation vacancy diffusivity	$0.07\overline{D}$	cm^2/s	Fitted
α, the dependence of $\phi_{f/s}$ on the applied voltage	0.4751	-	From Fig. 3.19
β, the dependence of $\phi_{f/s}$on pH	-0.0109	V	From Fig. 3.20
$w = \Delta G_{\mathrm{s}}^0 + \frac{\chi}{2}\Delta G_{\mathrm{A}}^0 - \frac{\chi}{2}F\phi_{f/s}^0$	21.107	kJ/mol	From Eq. 1.6
$\gamma' = \frac{\chi\alpha F}{2RT}$	9.34	V^{-1}	Calculated

It is important to note that the CPDs approach the potential axis asymptotically as the potential is made more negative and hence the probability is never zero, corresponding to the possibility that potential breakdown sites having very high cation vacancy diffusivities are present on the surface. According to King et.al. [23], the corrosion potential of a copper canister in a KBS-3 repository will increase with time from about -0.75 V_{SCE} (-0.505V_{SHE}) to -0.1 V_{SCE} (0.1444V_{SHE}) over the first hundred years of storage ("oxic" period), corresponding to an initial increase in the temperature of the canister surface from 74^{o}C to 90^{o}C after 20 years, due to the heat output of the decaying nuclear waste, followed by a decline in temperature to 34^{o}C after 100 years and finally to about 15^{o}C after 1,000,000 years of isolation [24]. The initial increase in the corrosion potential can be attributed to the increase in temperature for t < 20 years, in spite of the fact that the oxygen concentration also declines over the same period. Eventually, for 20 < t < 1,000,000 years the decline in oxygen concentration causes the corrosion potential to decline from -0.1V_{SCE} (0.1444V_{SHE}) to -0.99V_{SCE} (-0.746V_{SHE}), in spite of the fact that the temperature also continues to decline. While the present paper does not address the temperature dependence of the V_c (although see below), it is evident from a comparison of the calculated corrosion potential values of King et.al. [23] with the CPDs for V_c plotted in Figure 3.22(a) that pitting must be recognized as a potential threat to canister integrity, particularly at shorter times (t < 1000 years), but as stated later in this report inconsistencies in our calculated corrosion potential with that estimated by King et.al. [23] must be resolved before a meaningful comparison can be made.

4.4. Conclusions

Experimental relationships between the breakdown potential (V_c) and chloride activity and pH have demonstrated the validity of the Point Defect Model (PDM) for describing passivity breakdown on copper in chloride-containing sodium sulphide solutions. Analysis of the dependence of the breakdown potential on chloride activity and pH yield the value for the polarizability of the barrier layer/solution interface (α) and the dependence of the potential drop across the barrier layer/solution interface on pH (β).

The critical, areal cation vacancy concentration ξ leading to passivity breakdown on copper is of the order of 1.09×10^{15} cm^{-2}, as determined from the dependence of the apparent breakdown potential on the potential sweep rate, as given by the PDM. This is in excellent agreement with that (10^{14} -10^{15} cm^{-2}) estimated structurally, assuming vacancy condensation on either the copper substrate or on the cation sublattice of the barrier layer (Cu_2S).

The experimentally-determined, near normal distributions in the cumulative probability of the breakdown potential for different chloride concentrations are found to be in satisfactory agreement with theory in the quantitative characterization of the breakdown potential distributions for Cu as calculated from the PDM. Because the CPD approaches the abscissa asymptotically as the potential is reduced, there exists a finite probability that passivity breakdown might occur at a potential that is considerably more negative (perhaps by 200 or 300 mV), particularly in the light of the large surface area of a canister and the excessively long exposure time in the repository. Such breakdown sites would be characterized by abnormally high cation vacancy diffusivities.

4.5. References

1. H. H. Strehblow, Werkst. Korr., 27 (1976) 792.
2. M. Ergun, A. Y. Tutan, Pitting potential and protection potential of carbon steel for chloride ion and the effectiveness of different inhibiting anions, Corros. Sci., 32 (1991) 1137.
3. E. McCafferty, A Competitive Adsorption Model for the Inhibition of Crevice Corrosion and Pitting,J. Electrochem. Soc., 137 (1990) 3731.
4. D. D. Macdonald, The point defect model for the passive state, J. Electrochem. Soc., 139(12) (1992) 3434-3449.
5. P. Zaya, M.B. Ives, Proc. Natl. Res. Counc. Can., 135 (1984).
6. T. Shibata, 1996 Whitney Award Lecture: Statistical and stochastic approaches to localized corrosion, Corrosion, 52 (1996) 813.
7. H. H. Strehblow, B. Titze, Pitting potentials and inhibition potentials of iron and nickel for different aggressive and inhibiting anions, Corros. Sci., 17 (1977) 461.
8. D. D. Macdonald, Passivity: The key to our metals-based civilization, Pure Appl. Chem., 71 (1999) 951-986.
9. L. F. Lin, C. Y. Chao, D. D. Macdonald, A Point-Defect Model for Anodic Passive Films .1. Film Growth-Kinetics, J. Electrochem. Soc., 128 (1981)1194.
10. T. Haruna and D. D. Macdonald, Theoretical prediction of the scan rate dependencies of the fitting potential and the probability distribution in the induction time, J. Electrochem. Soc., 144 (1997) 1574-1581.
11. M. Urquidi-Macdonald, D. D. Macdonald, Theoretical Distribution-Functions for the Breakdown of Passive Films, J. Electrochem. Soc., 134 (1987)41.
12. D. D. Macdonald, E. Sikora, M. W. Balmas, R. C. Alkire, The photo-inhibition of localized corrosion on stainless steel in neutral chloride solution, Corros. Sci., 38(1996) 97.

13. C. B. Breslin, D. D. Macdonald, E. Sikora, and J. Sikora, Influence of UV light on the passive behaviour of SS316 - Effect of prior illumination, Electrochim. Acta, 42(1997) 127.
14. M. Urquidi, D. D. Macdonald, Solute-Vacancy Interaction-Model and the Effect of Minor Alloying Elements on the Initiation of Pitting Corrosion, J. Electrochem. Soc., 132 (1985) 555.
15. V. M .M. Lobo, Electrolyte solutions: Literature Data on Thermodynamic and Transport Properties, Coimbra, Portugal, 1984.
16. D. Dobos, Electrochemical Data: A Handbook for Electrochemists in Industry and Universities, Elsevier Scientific Publishing Company, Amsterdam-Oxford-New York, 1975.
17. I. T. E. Fonseca, N. Lima, J. A. Rodrigues, M. I. S. Pereira, J. C. S. Salvador, and M. G. S. Ferreira, Passivity breakdown of Al 2024-T3 alloy in chloride solutions: a test of the point defect model, Electrochem. Comm., 4 (2002) 353-357.
18. Y. Zhang, Determination of damage functions for the pitting of AISI type 403 blade alloy and ASTM A470/471 disk alloy, PhD Thesis, Penn State University, 2005.
19. Y. Zhang, D. D. Macdonald, M. Urquidi-Macdonald, G. Engelhardt, and R. B. Dooley, Passivity breakdown on AISI Type 403 stainless steel in chloride-containing borate buffer solution, Corros. Sci., 48 (2006) 3812-3823.
20. Z. Szklarska-Smialowska, Pitting Corrosion of Metals, NACE, Houston, Texas, 1986.
21. D. D. Macdonald, M. Urquidi-Macdonald, Distribution-functions for the breakdown of passive films, Electrochim. Acta, 31(8) (1986) 1079-1086.
22. D. D. Macdonald and M. Urquidi-Macdonald, Theory of Steady-State Passive Films, J. Electrochem. Soc. 137 (1990)2395-2402.
23. F. King, M. Kolar, M. Vähänen, and C. Lilja, Modelling the Long-Term Corrosion Behaviour of Copper in a KBS-3 Repository, Corros. Eng. Sci. Tech., 46 (2) (2011) 217-222.
24. F. King, C. Lilja, K. Pedersen, P. Pitkänen and Marjut Vähänen, SKB-TR-10-67, Svensk Kärnbränslehantering AB, (2010).
25. D. D. Macdonald, S. Sharifi-Asl, and G. R. Engelhardt, Issues in the Corrosion of Copper in a Swedish High Level Nuclear Waste Repository: Phase III. Role of Sulphide Ion in Anodic and Cathodic Processes, Technical Note 2014:57, Swedish Radiation Safety Authority, Sweden (2014).

5. Passivity Breakdown on Copper: Influence of Temperature

5.1. Introduction

The passivity of copper is the basis for its reliable use as the outer canister material for the disposal of high-level nuclear waste (HLNW) in Sweden and Finland. The breakdown of passivity is the principal reason for localized corrosion failures, such as pitting and stress corrosion cracking, in long-term service. The process yielding the breakdown of passivity and initiation of pitting corrosion on copper has been explained through the Point Defect Model (PDM), which is found to accurately account for passivity breakdown on this metal in simulated sulphide-containing granitic ground water at a constant temperature, as discussed in the previous section [1-4].

However, due to the nuclear reactions within the spent fuel, the temperature of the canisters is estimated to be about 80 - 90 °C during the first 100 - 200 years in the repository, and is then predicted to decrease to about 15°C during the first several thousands of years [5]. The temperature is predicted to evolve over 10,000 years as indicated in Figure 4.1. Of particular interest, for this analysis, is the temperature at the buffer inner surface, representing the interface between the copper and the environment. The temperature is predicted to increase over the first ten to twenty years of storage, corresponding to the placement of more canisters and the loss of convective air cooling as the tunnels are backfilled with a sand/bentonite mixture. At longer times, the temperature decreases as the various radioactive isotopes in the waste decay, such that after 10,000 years the temperature is predicted to be near ambient. In performing the Gibbs energy minimization calculations, we assume that the bentonite buffer is fully saturated with groundwater and that the conditions are anoxic. Attempts to perform Gibbs energy minimization for oxic conditions, where a significant concentration of oxygen was present, were unsuccessful as all of the pyrite was predicted to be consumed and the predicted pH was excessively low, corresponding to the oxidation of sulfur to sulfuric acid. Therefore, localized corrosion, especially pitting corrosion, should be considered during this period as occurring at elevated temperatures (ranging from 20ºC to 90ºC) [6, 7].

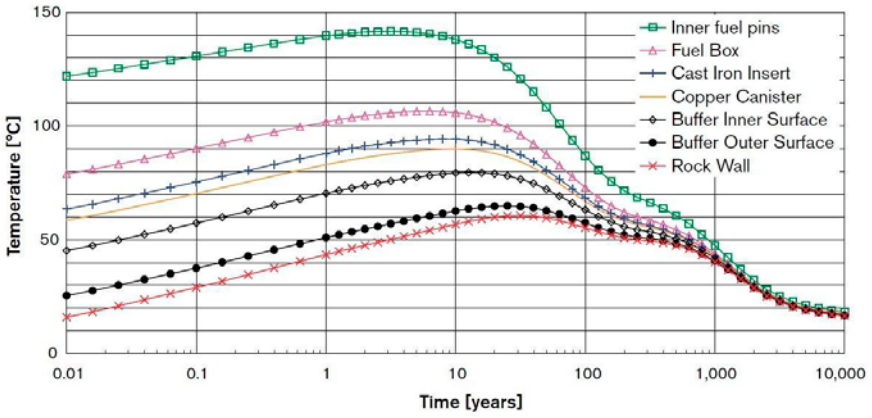

Figure 4.1. The thermal evolution for a number of locations in a canister at mid-height in a granitic repository [6].

On reviewing the literature on the pitting of copper in environments containing chloride ion and sulphide ion, we concluded that the available database is very limited [7, 8]. In point of fact, the available data on the effect of temperature on the thermodynamics and kinetics of pitting corrosion of copper is such that no meaningful predictions could be made and we therefore concluded that the required data must be measured experimentally. According to the previous study reported in the Phase II report [2], sulphide for the reaction, $2Cu + HS^- + H^+ \rightarrow Cu_2S + H_2$, the value of P^e rises by more than twenty-five orders of magnitude at ambient temperature for sulphide concentrations that are typical of the repository compared to the sulphide-absent case, demonstrating the powerful activating effect of sulphide ion on the general corrosion behaviour of copper, particularly at elevated temperature. However, we could find no clear evidence that sulphide ion induced passivity breakdown and it appears that this role is played by chloride ion, as is the case for metals with oxide barrier layers.

The work reported in this chapter studies the impact of temperature on the passivity of copper in sulphide-containing brines and in characterizing the susceptibility of copper to pitting corrosion in the same solutions as a function of temperature. Thus, this chapter reports the temperature- and chloride-dependencies of electrochemical parameters related to pitting corrosion of copper. On the other hand, as mentioned in literature [9-12], in order to predict the occurrence of stable pitting corrosion, it is necessary to know two characteristic parameters as functions of solution chemistry, i.e., the corrosion potential and the repassivation potential. The repassivation potential (E_{rp}) is a measure of the tendency of stable pits to die as the potential is displaced in the negative direction from the breakdown potential and is considered by some to be the more fundamental and important

of the two pitting potentials. The effect of pit growth on E_{rp} of copper was examined in the present work by using cyclic potentiodynamic polarization measurement.

5.2. Experimental

The electrochemical measurements were performed in a conventional three-electrode cell (double walled, in order to maintain constant temperature of the test medium with a water inlet and outlet connected to a thermostatic bath), using a working electrode (WE) made from pure copper rod (Puratronic®, 99.999% Alfa Aesar®). A saturated calomel electrode (SCE) and Pt plate were employed as reference electrode (RE) and counter electrode (CE), respectively. The reference electrode was connected to the cell through an electrolyte bridge/Luggin capillary probe.

The working electrode was mounted in epoxy resin with a 0.317 cm^2 area exposed to solution. The WE surface was abraded to a mirror finish with 600#, 800# and 1200# SiC paper and then further polished with 0.1μm diamond Polishing Suspension. After polishing, the electrode was rinsed with doubly distilled water and dried with pressurized nitrogen. The H_3BO_3/NaOH buffer system was chosen, because it not only provides the necessary conductivity and a stable pH, but also is the system that itself exerts the least influence on the surface properties of metals. The solution compositions are listed in Table 1. The pH of the buffer solutions was regulated to 9.0 by the concentration of NaOH. H_3BO_3 (≥99.5%, Sigma), NaOH (anhydrous, ≥98%, Sigma-Aldrich), Na_2S (monohydrate, ≥99.99%, Aldrich) and NaCl (anhydrous, ≥99%, Sigma-Aldrich) were used to prepare the solutions with double distilled water (18.3 MΩ cm^{-1}, mili-Q). The experimental temperatures were ambient temperature (22±2ºC) and elevated temperatures (42±1ºC, 62±1ºC and 82±1ºC).

Table 4.1. Composition of solutions (pH=9.0 ± 0.2)

No.	Composition
1	0.05M NaCl+2×10^{-4}M Na_2S+0.2M borate buffer
2	0.1M NaCl+2×10^{-4}M Na_2S+0.2M borate buffer
3	0.5M NaCl+2×10^{-4}M Na_2S+0.2M borate buffer
4	1.0M NaCl+2×10^{-4}M Na_2S+0.2M borate buffer
5	5.0M NaCl+2×10^{-4}M Na_2S+0.2M borate buffer

The solutions were purged with ultrahigh-purity N_2 gas (UHP, 99.999%) having a stated oxygen concentration of less than 1 ppm for about 2 h before the start of each experiment and also during all the experiments. The WE was initially reduced potentiostatically at -1.2 V vs. SCE for 5-min to remove any air-formed oxide on the surface of the electrode. A two-hour test of the open circuit potential (OCP) was

carried out before the potentiodynamic polarization (PD) measurement (scan rate = 0.1667mV/second). For cyclic potentiodynamic polarization (CPP) case, a faster backward scan (100mV/s) is applied for killing the stable pits that form and grow at potentials above the critical breakdown potential, V_c. The potentiodynamic experiments were typically repeated 20 times to obtain the statistical distribution of the critical breakdown potential (V_c). All electrochemical experiments were performed using a Solartron 1280B Electrochemical Measurement System and accompanied by CorrWare/CorrView.

After the PD measurements were completed, the micro morphology was observed and the pit depth was measured by using the digital confocal microscope VHX-2000 (Keyence).

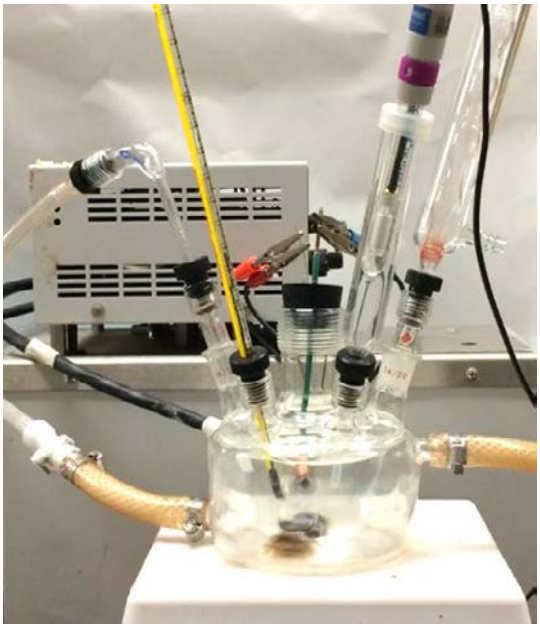

Figure 4.2. A photograph of the cell filled with borate buffer solution.

The scanning electron microscope (SEM, FEI Quanta250) with energy dispersive X-ray spectroscopy (EDS) was used to observe and analyze the sulphide film, which was first grown at different formation potentials (OCP, -600mV$_{SCE}$, -400mV$_{SCE}$, -200mV$_{SCE}$) in deaerated 1M NaCl and 2×10^{-4}M Na_2S solution (0.2M borate buffer, pH = 9.0 ± 0.2) at 40ºC for 24 hours, and then rinsed with deionized water and dried in the nitrogen gas flow.

5.3. Results and discussion

Typical potentiodynamic polarization curves for copper in deaerated borate buffer solutions (pH = 9±0.2) with constant concentration of Na_2S (2×10^{-4}M) and chloride (1M) as a function of temperature are shown in Fig. 4.3. The processes from active-to-passive, passive, and passivity breakdown can be identified in these polarization curves. Each polarization curve is characterized by a wide passive range terminating in a rise in the current density due to passivity breakdown at a potential that depends on the temperature. The measured critical breakdown potential of copper is seen to decrease with rising temperature, as is normally observed for passivity breakdown on other metals [13-15]. It is evident that temperature plays an important role in the passivity breakdown, because as the temperature increases the breakdown potential drops from around V_c=-0.24V_{SCE} at 22ºC to around V_c=-0.37V_{SCE} at 82ºC. The repeated potentiodynamic polarization curves and cumulative distributions for different temperatures are presented in Fig. 4.4 - 4.9.

Importantly, it is noted that the critical breakdown potentials measurements demonstrate the good reproducibility in this study. The distribution in V_c occurs over a range of potential of about 30mV, which is consistent with that reported in Chapter 3. From the results of the replicated experiments, the experiment-to-experiment fluctuations in the passive current density is also consistent with that reported in Chapter 3 for fixed chloride concentration.

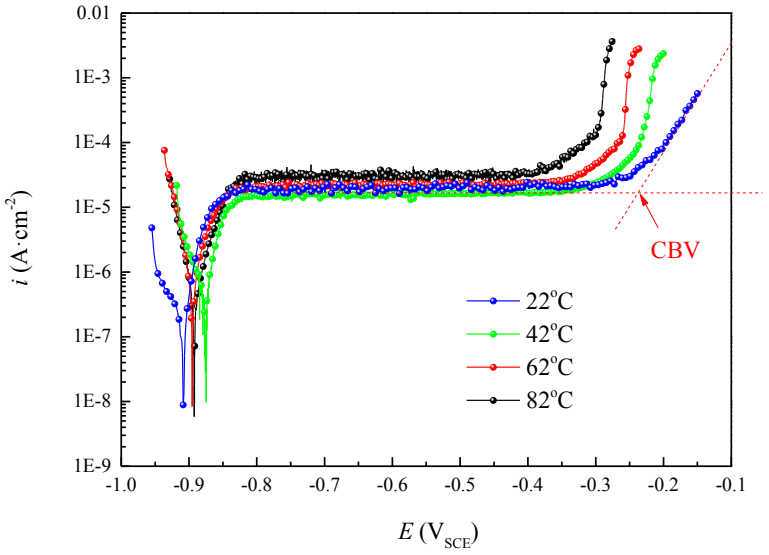

Figure 4.3. Typical potentiodynamic polarization curves for copper in deaerated 1M NaCl and 2×10^{-4}M Na_2S solution (0.2M borate buffer, pH = 9.0±0.2) as a function of temperature.

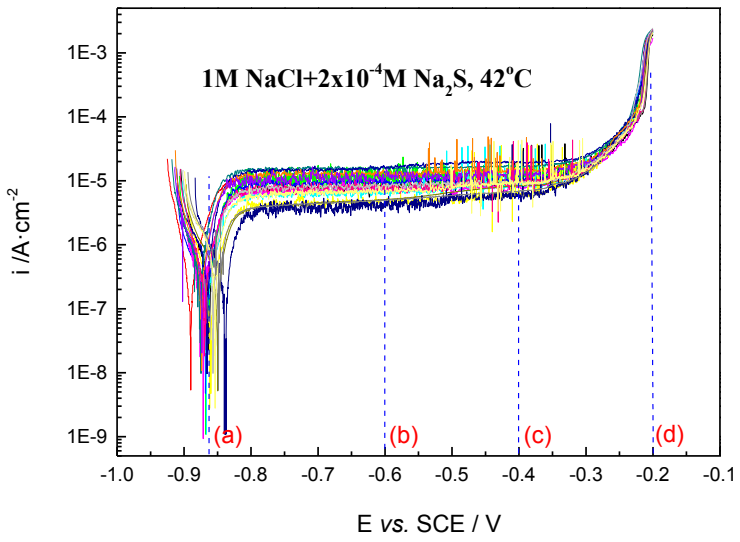

Figure 4.4. Potentiodynamic polarization curves of copper in in deaerated 1M NaCl and 2×10^{-4}M Na_2S solution (0.2M borate buffer, pH = 9.0±0.2) at 42 °C.

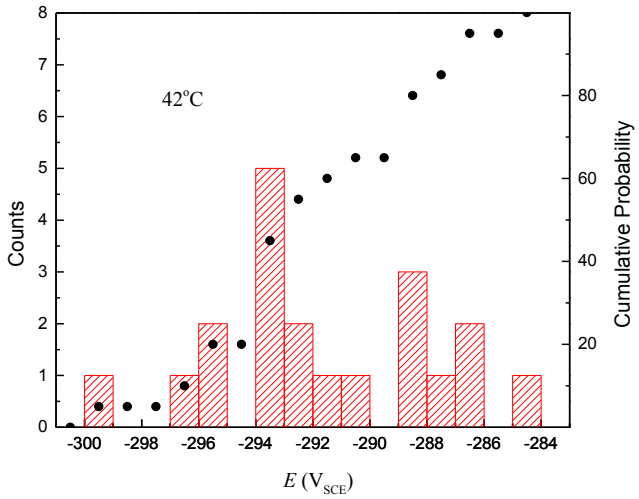

Figure 4.5. The statistics plot of V_c in deaerated 1M NaCl and 2×10^{-4}M Na_2S solution (0.2M borate buffer, pH = 9.0±0.2) at 42°C. The bars represent the "counts" (number of samples exhibiting breakdown within a 1 mV region) and the closed points represent the cumulative probability.

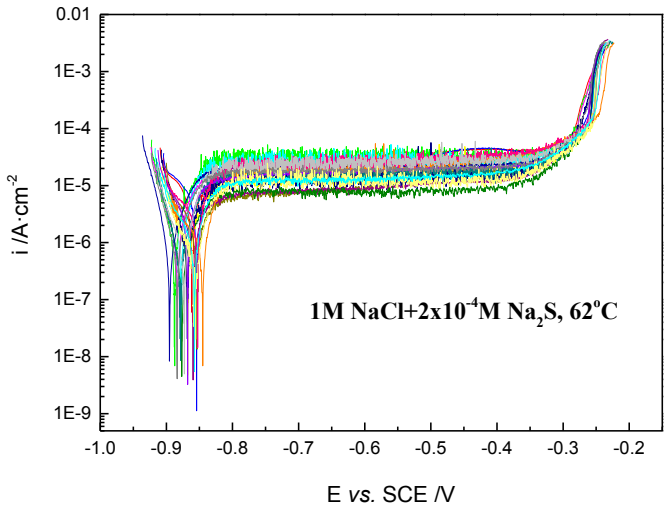

Figure 4.6. Potentiodynamic polarization curves of copper in deaerated 1M NaCl and 2×10^{-4}M Na_2S solution (0.2M borate buffer, pH = 9.0±0.2) at 62 °C.

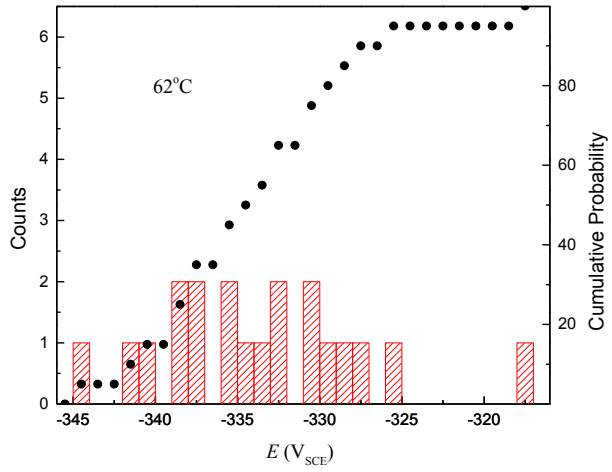

Figure 4.7. The statistics plot of V_c in deaerated 1M NaCl and 2×10^{-4}M Na_2S solution (0.2M borate buffer, pH = 9.0±0.2) at 62°C. The bars represent the "counts" (number of samples exhibiting breakdown within a 1 mV region) and the closed points represent the cumulative probability.

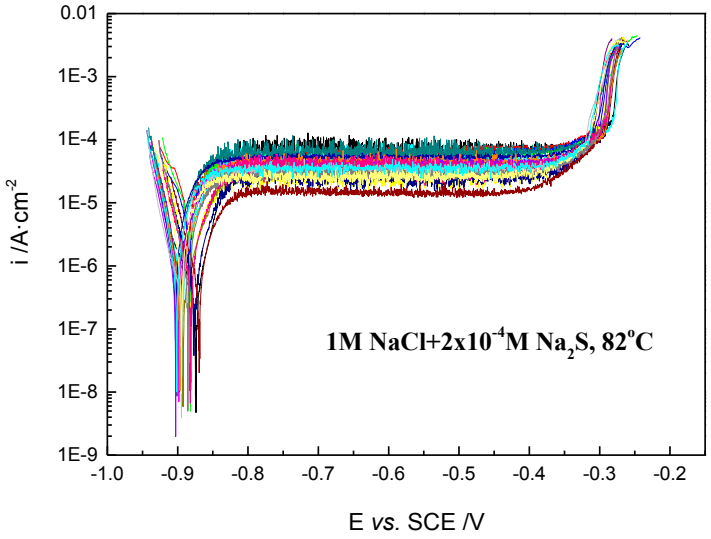

Figure 4.8. Potentiodynamic polarization curves of copper in deaerated 1M NaCl and 2×10^{-4}M Na_2S solution (0.2M borate buffer, pH = 9.0±0.2) at 82 °C.

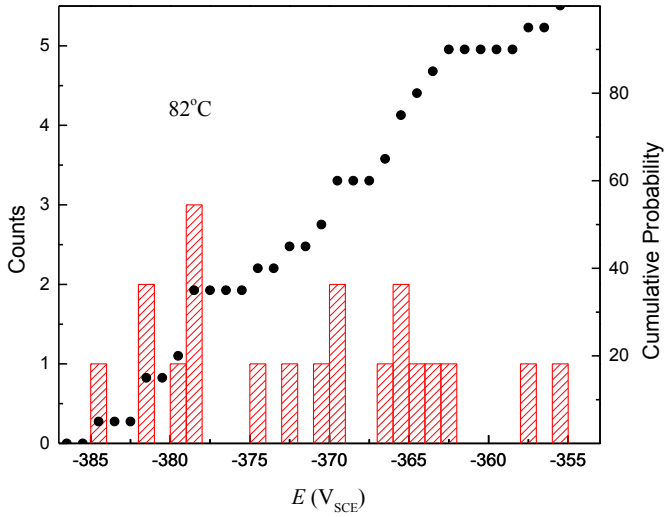

Figure 4.9. The statistics plot of V_c in deaerated 1M NaCl and 2×10^{-4}M Na_2S solution (0.2M borate buffer, pH = 9.0±0.2) at 82°C. The bars represent the "counts" (number of samples exhibiting breakdown within a 1 mV region) and the closed points represent the cumulative probability.

Due to the time limitations, the critical breakdown potentials for other chloride concentrations (0.05M, 0.1M, 0.5M and 5.0M) at different temperatures were only obtained from three separate measurements using a potential sweep rate υ = 0.1667mV/s. Once the difference of any two breakdown potentials in the repeated separate measurements

exceeded 20mV, the experiment was then repeated. Based on Equation (4.1) from the PDM [16-18], the breakdown potentials at each chloride concentration appears to decrease linearly with $\log(a_{Cl^-})$. The linear slope of the CBV (v = 0.1667mV/s) versus $\log(a_{Cl^-})$ can be used to determine the value of α.

$$V_c = V_0 - \frac{\beta}{\alpha}\text{pH} - \frac{2.303RT}{\alpha F}\log[a_{Cl^-}] \quad (4.1)$$

where α is the polarizability of the f/s interface [i.e. the dependence of the potential drop ($\emptyset_{f/s}$) across the barrier layer/outer layer/solution interface on the applied potential] and β is the dependence of the potential drop across the barrier layer/solution interface on pH, both can be determined by measuring V_c as a function of chloride concentration (activity) and pH, respectively.

The critical breakdown potential at elevated temperature (42 ºC, 62 ºC and 82 ºC) also appears to decrease linearly with $\log(a_{Cl^-})$ (Figure 4.10). The linear relationship becomes gradual with increasing temperature.

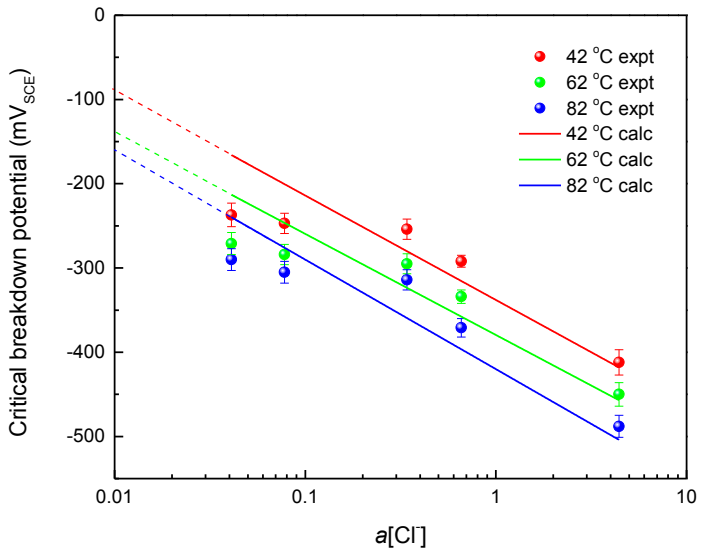

Figure 4.10. The mean in distribution in the critical breakdown potential as a function of chloride ion activity at different temperature.

Table 4.2. The linear slopes of V_c (v = 0.1667mV/s) ~ log(a_{Cl^-}) for copper in deaerated solutions (pH = 9.0 ± 0.2) at different temperatures

Temperature		Slope (V)	α
(ºC)	(K)		
42	315.1	-0.124	0.50
62	335.1	-0.120	0.55
82	355.1	-0.130	0.54

By using Equation (4.1), the value of α at each temperature is computed from the respective slope (Table 4.2). Compared with the result obtained at room temperature (Table 3.2), the α value shows a slight increase as the temperature increases. The temperature dependence of α can be related, in principle, to the properties of the barrier layer/solution interface at the different temperatures. From the EIS results in Phase III [3], one expected impact of increasing temperature is an increase in the porosity and/or dissolution of the sulphide passive film (barrier or outer layers), but the experimental results are not consistent with this expectation. Therefore, we can conclude that the value of α is only weakly dependent upon temperature. Generally, the voltage drop across the film/solution interface is linearly dependent upon the applied voltage and the pH, i.e. [16].

$$\emptyset_{f/s} = \alpha V + \beta pH + \emptyset^0_{f/s} \qquad (4.2)$$

where α is the polarizability of the film/solution interface, β is the dependence of the voltage drop across the f/s interface on pH, and $\emptyset^0_{f/s}$ is the value of $\emptyset_{f/s}$when V = 0 and pH = 0. When the applied voltage and pH values of solution are same, the voltage drop across the film/solution interface at elevated temperature (such as 62ºC) is larger than that at ambient temperature.

The surface of the copper sulphide film, which was formed in deaerated 1M NaCl and 2×10^{-4}M Na_2S solution (0.2M borate buffer, pH = 9.0 ± 0.2) at different formation potentials (OCP, -600mV$_{SCE}$, -400mVSCE, -200mVSCE) at 40ºC, was examined by EDS. Figure 4.11 shows the elements maps of sulphide film on copper. As can be seen, Cu, S, O and Cl were detected within the film section. It is apparent that the sulphide film was not homogenous as initially concluded in the Phase III report [3]. As the potential shifts from OCP toward -400 mV$_{SCE}$ the thickness of sulphide film increases. There is little chloride in the passive film when the potential is more negative than the critical breakdown voltage (CBV) [Figures 4.11 (a), (b) and (c)].

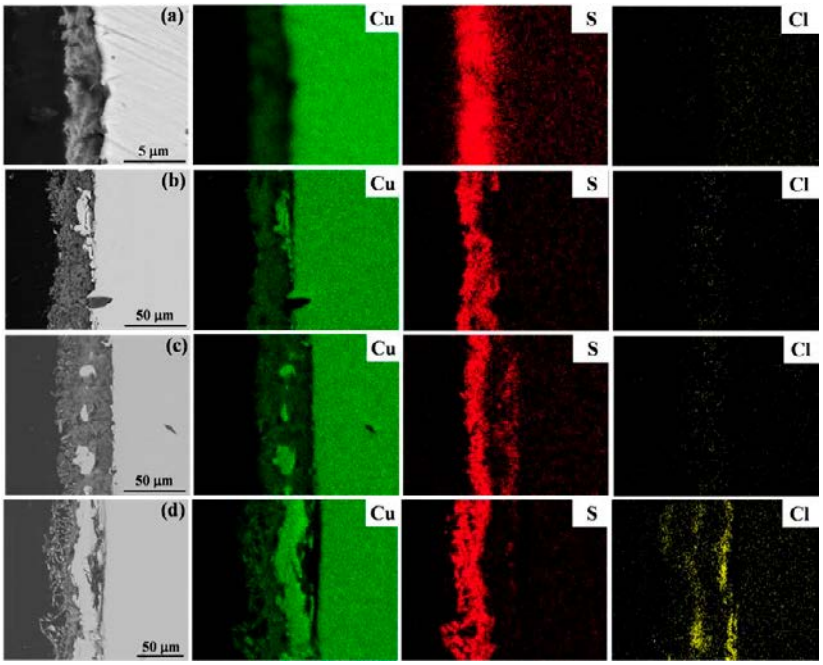

Figure 4.11. Film section EDS maps of copper at different film formation potentials for 24 h in deaerated 1M NaCl and 2×10^{-4}M Na_2S solution (0.2M borate buffer, pH = 9.0±0.2) at 40 ºC: (a) OCP, (b) -600 mV_{SCE}, (c) -400 mV_{SCE}, (d) -200 mV_{SCE}

It has been suggested that metal sulphides oxidize to form elemental sulfur [19] and also that they chemically dissolve to form H_2S [20]. Many different forms of dissolved sulfur species can decrease the pitting potential of stainless steel in chloride solutions [21], and it has been suggested that sulfur can enrich at the surface to lower the activation energy for dissolution and inhibit passivation [22]. From Figure 4.11(d), the enrichment of both sulfur and chlorine occurs in the surface film when the film formation potential is approximately +90mV over the critical breakdown potential. Based on the previous literature and experiment results, the 'Synergy Effects' on pitting corrosion may exist in simulated HLNW repository environment.

Based on PDM [23], the breakdown potential (V_c) has been found previously to increase linearly with the square root of potential sweep rate ($v^{1/2}$, positive direction) under potentiodynamic polarization conditions, as described previously in this report. In any event, the measured breakdown voltage may be corrected to zero scan rate as described by the equation:

$$V_c(v) = \left(\frac{2\xi RT}{\chi\alpha F J_m}\right)^{1/2} v^{1/2} + V_c(v=0) \qquad (4.3)$$

where V_c (v=0) is defined as the breakdown potential at zero potential scan rate. Employing the value of α determined earlier and the ratio

of (ξ/J_m) [15, 23] as obtained from the slope of V_c versus $v^{1/2}$ (see Fig. 4.12) the value of ξ is estimated after the approximation of J_m based on its relationship with J_{ca}, as noted previously in this report. From previous work, J_m is less than 6.24×10^{13} cm^{-2}/s. The value of ξ, which is the critical areal (two-dimensional) concentration of condensed vacancies at the metal/barrier layer interface, can be determined. ξ is therefore less than $1.04\times10^{15}cm^{-2}$, $1.14\times10^{15}cm^{-2}$, $1.11\times10^{15}cm^{-2}$ at 42, 62, 82ºC, respectively; that is, ξ does not change with temperature. This result is in keeping with expectation, because ξ is a structurally-determined parameter and it is not expected that the lattice constants of the barrier layer will change appreciably with temperature over the 22°C to 82°C range.

The critical areal cation vacancy concentration ξ that leads to passivity breakdown can also be calculated from the unit cell dimension of the metal and the barrier layer, and hence can be compared with the value estimated above from the potential sweep rate dependence of the breakdown potential [24]. From the previous discussion in Chapter 3, the estimated areal atomic density of Cu/Cu_2S is, respectively, $1.53\times10^{15}cm^{-2}$ in the metal and $7.66\times10^{14}cm^{-2}$ in the barrier layer. Therefore, the value estimated for ξ from the relationship between $V_c(\upsilon)$ and $v^{1/2}$ is in close agreement with that calculated from the geometric structure of the metal/barrier layer (Cu/Cu_2S) system. It appears that the cation vacancy condensation probably occurs on the cation sublattice of the barrier layer, but condensation on the substrate metal lattice cannot be ruled out unequivocally. The result provides powerful evidence for the validity of the PDM in describing passivity breakdown of copper in simulated HLNW ground water.

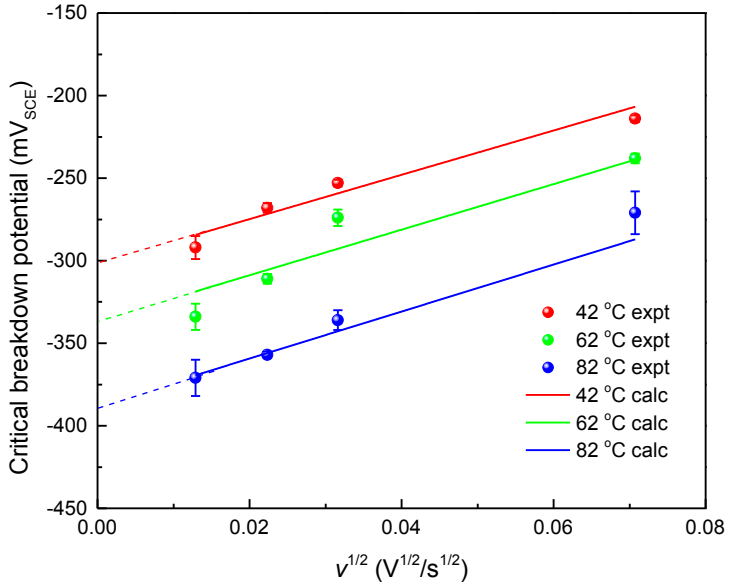

Figure 4.12. The measured breakdown potentials (V_c) at different potential scan rates (v) for Cu in 1.0M NaCl + 2×10^{-4}M $Na_2S\cdot9H_2O$ solutions at different temperature.

By using Eqs. (3.6)-(3.8), and the parameter values extracted from the above experiments (Table 4.3), the statistical distribution in the breakdown potential for copper in deaerated sodium sulphide solution (pH = 9 ± 0.2) at different temperature can be calculated. The calculated distributions using $\sigma_D = 0.07\overline{D}$ are plotted in Fig. 4.13 as cumulative probabilities in the breakdown potential, and are compared with the experimental distributions in the breakdown potential obtained from the potentiodynamic experiments performed in this study. In order to obtain statistically valid distributions, these experiments were repeated 20 times, at least. The marked points are experimental data while the solid lines correspond to the calculated distributions. When the temperature changes from 22ºC to 82ºC, the experimental distributions are narrow, and hence in good agreement with the calculated distribution functions with a small $\sigma_D = 0.07\overline{D}$. In any event, the experimental distributions in the breakdown potential are in satisfactory agreement with those calculated from the PDM with $\sigma_D = 0.07\overline{D}$.

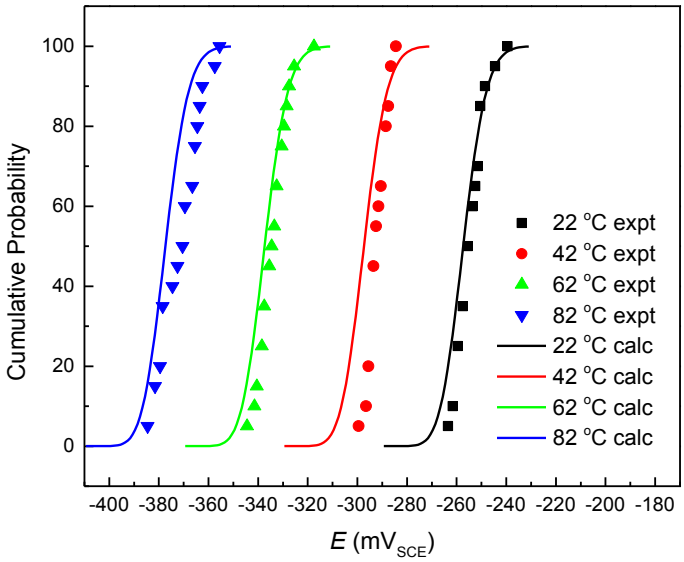

Figure 4.13. Calculated cumulative probabilities in the breakdown potential for Cu in 1.0M NaCl + 2×10^{-4}M $Na_2S\cdot9H_2O$ (pH = 9±0.2) at different temperature, compared with the experimentally-determined distributions.

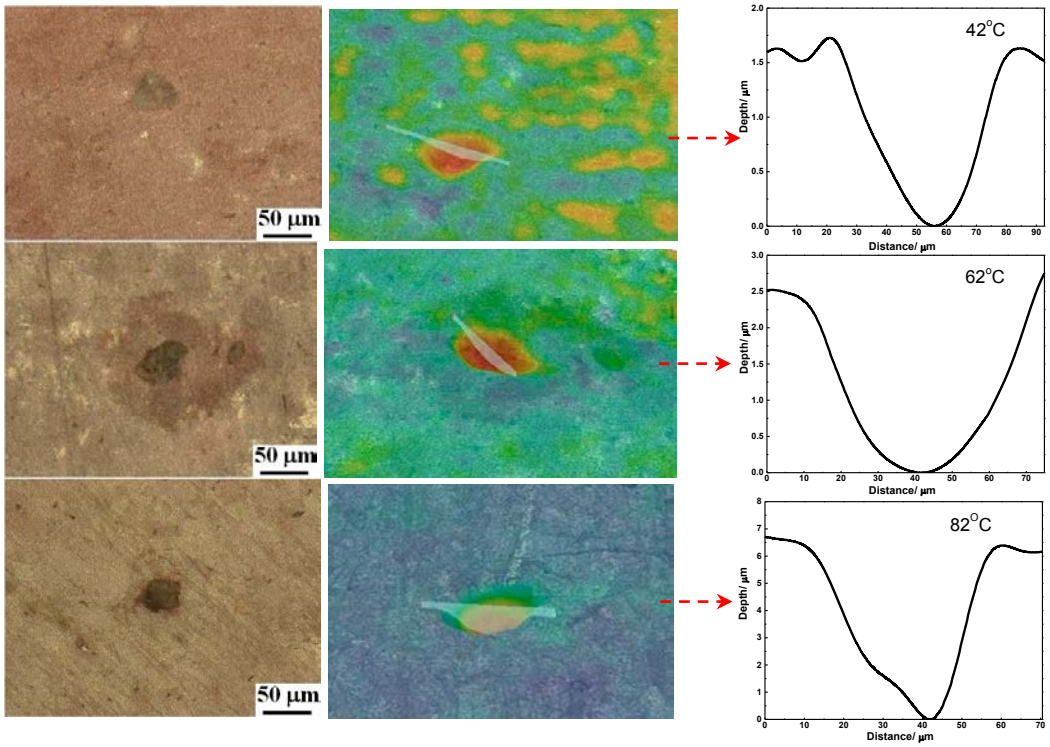

Figure 4.14. Photographs of copper surface and pits size data after potentiodynamic polarization measurement in 1.0M NaCl + 2×10^{-4}M $Na_2S\cdot9H_2O$ (pH = 9±0.2) at different temperature.

Table 4.3. Parameter values used in calculating cumulative probabilities in the critical breakdown potential for copper in deaerated sodium sulphide solution (pH = 9±0.1) at different temperature

Parameter	Value	Units	Source
T, the absolute temperature	315.1	K	Defined
	335.1		
	355.1		
χ, the barrier layer stoichiometry (Cu_2S)	1	-	Assumed
Ω, molar volume of Cu_2S per cation	28.42	cm^3/mol	From density
ε, the electric field strength	5×10^6	V/cm	Assumed
J_m, the rate of annihilation of cation vacancies at the metal/film interface	6.24×10^{13}	$No./(cm^2s)$	From chapter 3
ξ, the critical areal cation vacancy concentration	1.04×10^{15} (at 315.1 K)	$No./cm^2$	From Fig. 4.12
	1.14×10^{15} (at 335.1 K)		
	1.11×10^{15} (at 355.1 K)		
$\overline{D}$, the mean cation vacancy diffusion coefficient	4.22×10^{-13}	cm^2/s	Ref. 3
σ_D, the standard deviation for the cation vacancy diffusivity	$0.07\overline{D}$	cm^2/s	From Fig. 4.13
α, the dependence of $\phi_{f/s}$on the applied voltage	0.50 (at 315.1 K)	-	From Fig. 4.10
	0.55 (at 335.1 K)		
	0.54 (at 355.1 K)		
β, the dependence of $\phi_{f/s}$on pH	-0.0109	V	From chapter 3
$w = \Delta G_S^0 + \frac{\chi}{2}\Delta G_A^0 - \frac{\chi}{2}F\phi_{f/s}^0$	18.880 (at 315.1 K)	kJ/mol	From Eq. 1.6
	19.599 (at 335.1 K)		
	20.761 (at 355.1 K)		
$\gamma' = \frac{\chi\alpha F}{2RT}$	9.29 (at 315.1 K)	V^{-1}	Calculated
	9.60 (at 335.1 K)		
	8.86 (at 355.1 K)		

The VHX-2000 (Keyence) confocal microscope is an effective and easy-to-use tool for observing the uneven surface and measuring the pit depth, because it can compile images at different focal planes by using the Z-axis motorized stage.

Figure 4.14 displays the microscopic observations of typical pits after potentiodynamic polarization. The pit develops and becomes deeper (~1.8μm, 2.5μm, 6.9μm at 42ºC, 62ºC, 82ºC, respectively) with increasing solution temperature. Due to the complex nature of pit nucleation and pit growth, the experimental damage function cannot be obtained from the present data. We recommend that it be studied in future work.

Figure 4.15 shows typical cyclic potentiodynamic polarization (CPP) scans measured on copper in the simulated repository environment. It can be seen that there exists positive hysteresis when the potential is scanned back from above the breakdown potential, providing clear evidence of pitting corrosion. In order to obtain pits of different depths, the potential was held for different times (0-200s) at the breakdown potential or was held at different potentials above the breakdown value (0-30mV) for a single time (10s). Here, we define the repassivation potential as a cross-over potential of the forward and reverse scans [25] (see arrows in Figure 4.15). In order to explore the relationship between pit growth and the repassivation potential, it is necessary to integrate the localized corrosion current *vs*. time data (see Figure 4.16) to determine the charge, which is related to pit depth.

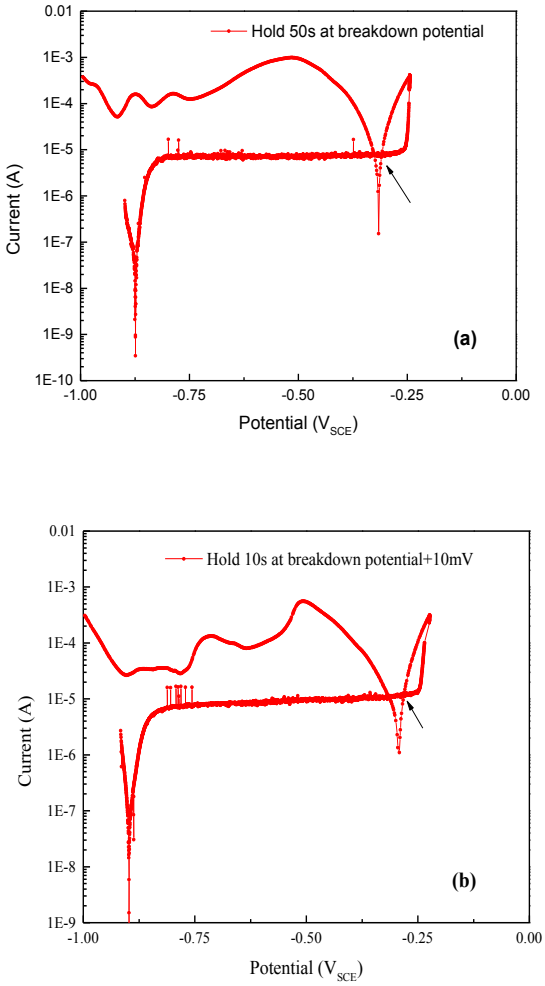

Figure 4.15. Cyclic potentiodynamic polarization curves for copper in 1.0M NaCl + 2×10^{-4}M $Na_2S\cdot9H_2O$ (pH = 9±0.2) at 62°C (v= 0.1667 mV/s), (a) Hold 50s at breakdown potential, (b) Hold 10s at breakdown potential+10mV. The arrow indicates the repassivation potential.

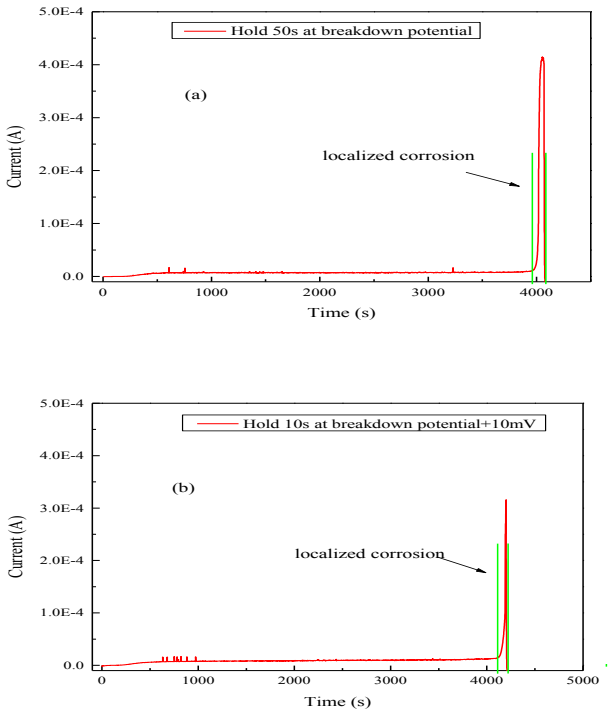

Figure 4.16. Current vs. time curves for copper in 1.0M NaCl + 2×10^{-4}M $Na_2S\cdot9H_2O$ (pH = 9±0.2) at 62°C (v= 0.1667 mV/s), (a) Hold 50s at breakdown potential, (b) Hold 10s at breakdown potential+10mV.

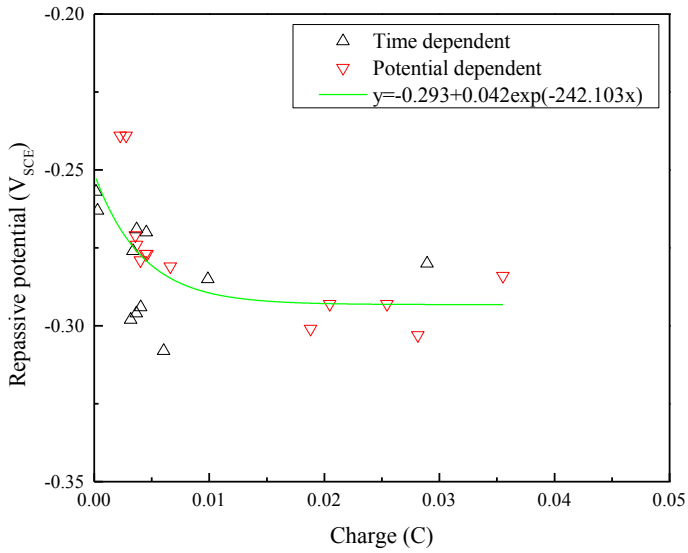

Figure 4.17. Effect of applied charge during pit growth on the repassivation potential of copper in 1.0M NaCl + 2×10^{-4}M $Na_2S\cdot9H_2O$ (pH = 9±0.2) at 62°C (v= 0.1667 mV/s).

The effect of the localized corrosion charge on the repassivation potentials for copper at 62°C is shown in Figure 4.17. The repassivation potential attains a lower-bound value with increasing pit charge, suggesting that E_{rp} could be a good indicator of localized corrosion performance. Thus, as shown in Figure 4.17, the same results are obtained whether pit size is varied by changing the hold time at constant potential or by varying the over-potential for a fixed time. This feature is confirmed by examining pit depth using the confocal microscope, as described earlier in this chapter.

Finally, the importance of the repassivation potential is that it marks the boundary below which a stable (macroscopic) pit cannot continue growing and, hence, as noted above, is regarded by some researchers as being the more fundamental and useful of the two pitting potentials. In the case of copper in the indicated environment, a pit, once nucleated, will continue to grow at potentials below V_c and above E_{rp}, but if the potential is displaced below E_{rp}, the pit instantly dies and no longer contributes to the evolution of localized corrosion damage on the surface. The difference, V_c - E_{rp}= 50mV, in the case of copper in the simulated repository environment, is relatively small (50 – 75 mV) compared with that for stainless steels in chloride-containing environments (typically hundreds of millivolts) [26-28], in keeping with the lower thermodynamic activity of Cu compared with the stainless steels.

5.4. Preliminary Consideration of the Evolution of Localized Corrosion Damage

Integral damage functions (IDFs) were calculated from the parameter values derived in this study for the pitting of copper in sulphide- and chloride-containing granitic ground water using Damage Function Analysis (DFA) [1], which includes a deterministic pit growth model, and are shown in Figure 4.18 for four exposure times (1, 6, 12 and 24 hours). The importance of the damage function is that it readily defines “failure”. Thus, if the system is characterized by a critical dimension of 10 μm, then failure would not have occurred after 1 hour exposure, but would have occurred after 5 hours of exposure, because, in that case, the deepest pit (10.4 μm) extends beyond the critical dimension. It is evident, therefore, for the purpose of predicting failure and maximum damage (penetration), that we are mostly interested in the behaviour of the upper extreme of the damage function. This interest is best expressed in terms of extreme value statistics (EVS) [1]; the empirical form of which has been used by many authors over many years to interpret empirical data. However,

in EVS, the two most important parameters, the shape and location parameters, must be determined empirically from the measurement of the distribution in the deepest pits on multiple specimens of the same area. This requires, essentially, "knowing the answer in advance" and hence EVS is fundamentally non-predictive, but does have some veracity for extrapolation. We have, however, derived from the PDM equations for the location and shape parameters that are the basis of Deterministic Extreme Value Statistics (DEVS) [1], which renders the method highly predictive.

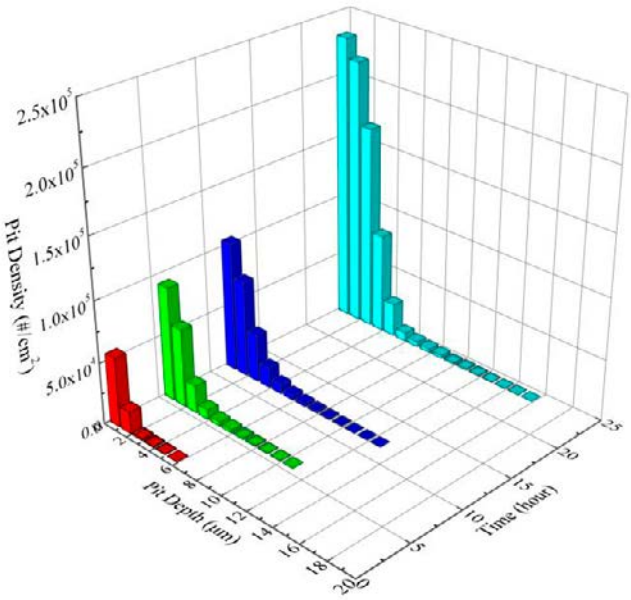

Figure 4.18. Pitting depth distributions ("integral damage functions") for copper in 1M Cl^- and 2×10^{-4}M S^{2-}, pH = 9 borate buffer at 60mV lower than breakdown potential for different times (V_c = -0.05 V_{SHE}). Note that it is difficult to measure the depth and number pits with depths of < 2μm, because of the resolution of a laser confocal microscope. Accordingly, pits with small depths are under-countered, but we are more interested in the pits with large depths, because they pose the most immediate threat to canister integrity.

An important finding of our research on pitting corrosion in copper in simulated granitic rock ground water, and for other metals and alloys in other systems [1], is that the penetration of the deepest pit does not increase linearly with time, but, instead trends toward a limiting value, as shown in Figure 4.19. This trend occurs, because, as time goes on, more and more of the active pits repassivate by a process known as "delayed repassivation". The origin of this phenomenon is well-understood in terms of the failure of a "stable pit" to maintain differential aeration, most commonly because the external surfaces fail to provide the resources in terms of oxygen reduction that are

necessary to maintain separation between the local anode (within the pit) and the local cathode (on the external surfaces). As a consequence, the pit cannot maintain the necessary, aggressive conditions (low pH, high [Cl^-]) within the enclave, and the aggressive solution disperses by diffusion into the bulk solution. If that occurs, the pit dies and the pit no longer grows into the substrate. Accordingly, the depth of the deepest pit trends toward a constant value. We have found this to be the case for every pitting system that we have ever studied [1], and we expect it to be the case for the pitting of copper in simulated repository ground water, as well, thereby limiting the damage that will accrue to the copper canisters in Sweden's proposed granitic rock repository.

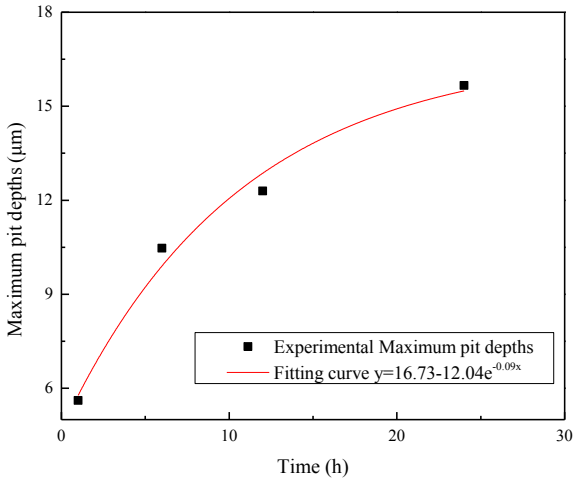

Figure 4.19. Maximum pit depths with exposure time for copper in 1M Cl^- and 2×10^{-4}M S^{2-}, pH=9 borate buffer at 60mV lower than breakdown potential for different time (V_c = -0.05 V_{SHE}).

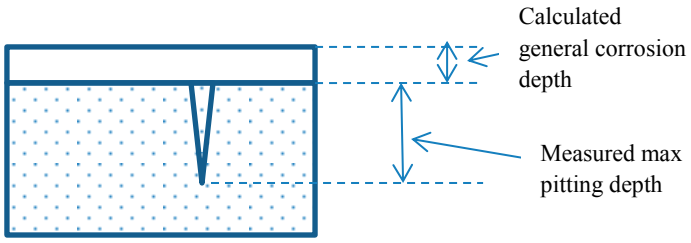

Figure 4.20. Pitting factor, which is defined as the measured maximum pitting depth + general corrosion depth divided by the general corrosion depth, as depicted in this plot.

Another important finding is the pitting factor is higher than one would normally expect. The pitting factor is calculated from the maximum pit depth and the general corrosion loss as depicted in Figure 4.20 and Equation 4.5.

Thus, from Faraday's law, we can derive the general corrosion depth (metal loss) as:

$$\text{General corrosion depth} = \frac{\int idt \times \Omega}{\delta F} \qquad (4.4)$$

so that the pitting factor becomes

$$Pitting\ Factor = MPD.\delta F / \int idt \times \Omega \qquad (4.5)$$

where *MPD* is the maximum pit depth, i is the passive current density (A/cm^2) at passivity breakdown, t is time (s), Ω is the mole volume per cation of the barrier layer of the passive film (cm^3/mol), δ is valence of copper ions in solution, and F is Faraday's constant (C/mole of electrons). It is considered that Cu^+ does not oxidize to Cu^{2+} in this case, because of the very low corrosion potential that is predicted to develop during the anoxic phase of waste storage in the repository (Figure 4.21). Thus, during this phase, the redox potential is so low that Cu^{2+} will not exist.

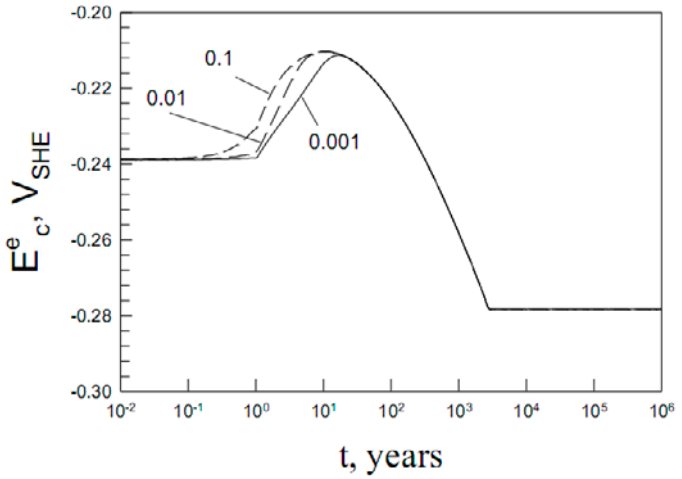

Figure 4.21. Equilibrium potential of the hydrogen electrode reaction as a function of time for different values of the bentonite porosity for pH = 8. As was previously shown, this value practically coincides with the corrosion potential of the copper canister in the repository. [1]

Comparison of the calculated corrosion potential data displayed in Figure 4.21 with those predicted by King [23] shows poor agreement and it is not entirely clear at present why this is so. One important factor is that King considered a lower sulphide concentration ($5x10^{-6}$ M) than that considered here (10^{-5} M) and, because of the strong activating effect of sulphide on copper (see Figures 1.2(a) and (b), the kinetics of the partial anodic process ($2Cu + HS^- \rightarrow Cu_2S + H^+ + 2e^-$) are expected to be greatly affected by the higher sulphide concentration in our work compared with King et.al. [23]. A second important difference is that King et.al. [23] regard the reduction of bisulphide (HS^-) as the appropriate cathodic partial reaction ($HS^- + e^- \rightarrow 1/2H_2 + S^{2-}$). However, we regard this to be incorrect as the bisulphide concentration ($5x10^{-6}$ M) is so low that the more likely cathodic reaction is the reduction of water ($H_2O + e^- \rightarrow OH^- + 1/2H_2$) for the same reason that hydrogen evolution from aqueous solutions is generally attributed to the reduction of H^+ for pH < 4 but for pH > 4, the species being reduced is H_2O; this is because the concentration of water is very much greater than that of H^+ at the higher pH, and the same conditions is likely to hold for HS^-. This postulate is confirmed by the work of Macdonald et.al. [3], who found that low sulphide concentration ($\leq 2\times10^{-5}$ M Na_2S) had little impact on the kinetics of hydrogen evolution on copper, but at higher concentrations, the rate of hydrogen evolution was clearly dependent on [HS^-]. These data argue strongly that both the reduction of HS^- and the reduction of H_2O must be considered when describing the corrosion of copper in the presence of sulphide ion in the repository environment within the concentration range of 0 to 10^{-5} M. Accordingly, the comparison is not included here, because these and other sources of the disagreement must be identified and corrected before a rational comparison between the corrosion potential and the pitting potential can be made.

Figure 4.22 and 4.23 show that the pitting factor is predicted to decrease exponentially with time. The exponential fitting curve shows that as time tends to infinity the pitting factor is decrease from 9.9 to 4.4 for the three applied potentials studied in this work. This is due to the fact that the maximum pit depth is a strong function of the applied potential, as it is with most metals and alloys, whereas the general corrosion loss is a much weaker function. However, the pitting factor is affected more obviously by temperature, with the long-term pitting factor increasing from 5.6 to 14.0 as the temperature increases from 42 ^{o}C to 82 ^{o}C (Figure 4.23). The importance of the pitting factor is clear; The expectation is that the pitting factor will continue to decrease with time if, for no other reason, the maximum pit depth approaches a time-independent value, but we do not know this for sure. The results show that there could be conditions for pitting to occur and hence it must be explored carefully.

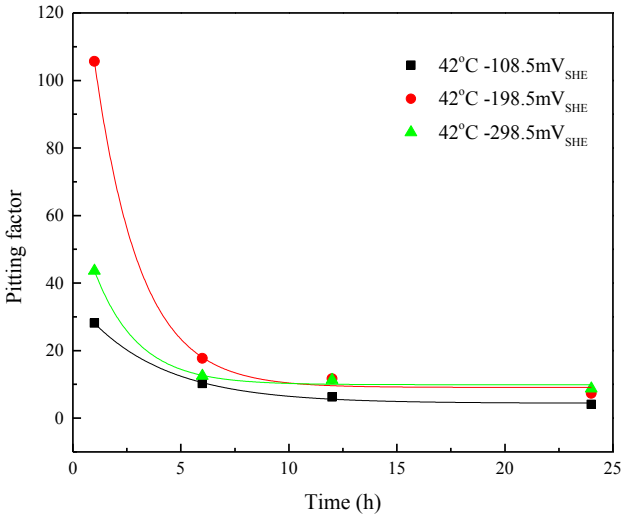

Figure 4.22. The pitting factor vs. time plot for copper in 1M Cl^- and 2×10^{-4}M S^{2-}, pH = 9 borate buffer at different applied potentials.

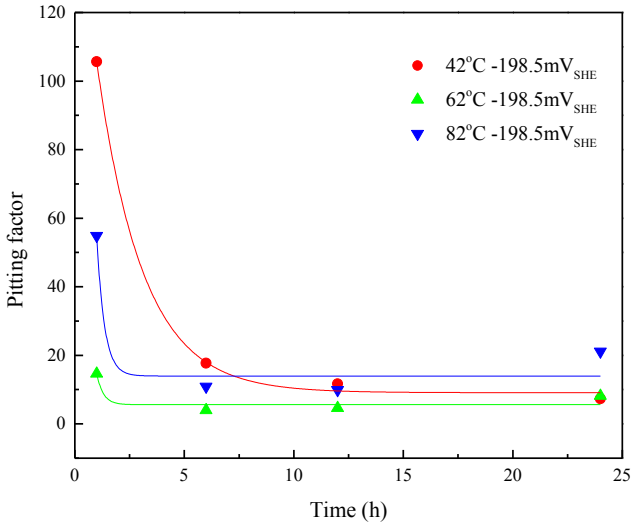

Figure 4.23. The pitting factor vs. time plot for copper in 1M Cl^- and 2×10^{-4}M S^{2-}, pH = 9 borate buffer at different temperatures and at an applied potential of -198.5mV$_{SHE}$.

The principal output of applying DEVS to copper would be plots like those shown in Figure 4.19, but extending to the longer exposure time periods corresponding to the repository conditions, as a function of [Cl^-], potential, and temperature. The maximum depth will be calculated theoretically using Deterministic Monte Carlo Simulation (DMCS) [1], which is also part of DFA, but which does not require calibration on short term, empirical data. Any empirical data that

might be available (e.g., from the literature or from experiments performed as part of a Phase V program) can be used to test the predictions of the model. Once these curves are known, then the risk of failure is readily assessed from the average depth of the deepest pit and the associated standard deviation.

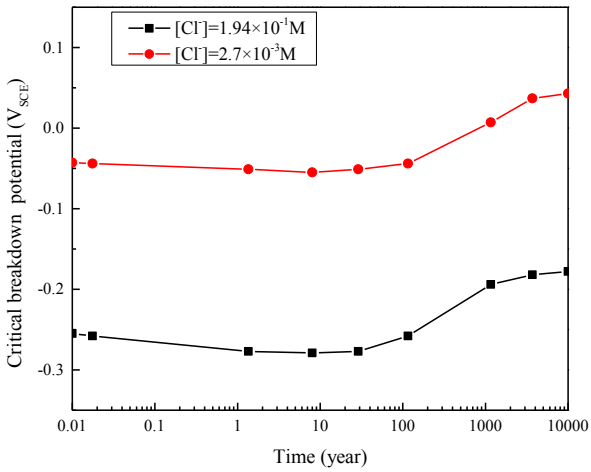

Figure 4.24. Predicted variation of critical breakdown potential with time of copper canister according to the thermal evolution [See Figure 4.1]. The black line and the red line indicate the critical breakdown potential in the condition with the upper bound of and the lower bound of chloride concentration in the groundwater estimated within the SR-Can project.

Finally, the predicted temperature versus time, which defines the corrosion evolutionary path for the repository, is expected to have a significant impact of the pitting of copper over the exposure history of the canisters. From the pitting potential versus temperature data shown in Figure 4.13 and from the temperature versus time data (Figure 4.1), we have tentatively constructed a plot in Figure 4.24 of how the pitting potential will change as the canister transitions along the corrosion evolutionary path. One can see that the pitting potential is low during the thermal period (t < 100 years), but for longer times the pitting potential is predicted to significantly increase thereby indicating a lower risk of pit nucleation. However, the variation of the pitting potential with time shown in Figure 4.24 (approx. 100 mV) is not so much larger than the dispersion in the breakdown voltage itself (approx. 30 mV, Figure 4.13) that the possibility of pitting can be discarded *a priori*. In this regard, it is important to note that the distributions displayed in Figure 4.13 approach the abscissa asymptotically, so that a finite cumulative probability of passivity breakdown will exist at voltages that are significantly below the mean, particularly when the long exposure times and large canister surface area are considered.

5.5. Conclusions

The corrosion behaviour of pure copper in a deaerated sodium chloride solution containing sulphide ion has been studied as a function of solution temperature by means of potentiodynamic, cyclic voltammetry, and potentiostatic polarization, as well as by SEM/ EDS. The findings of this work are summarized as follows:

- Pitting corrosion is observed on copper at elevated temperatures in simulated sulphide- and chloride-containing granitic rock groundwater where cuprous sulphide (Cu_2S) comprises the barrier layer of the passive film. The results show that increasing temperature decreases the mean breakdown potential.

- Experimental relationships between the breakdown potential (V_c) and temperature are readily accounted for by the Point Defect Model (PDM) for describing passivity breakdown on copper in chloride-containing sodium sulphide solutions. Analysis of the dependence of the breakdown potential on chloride concentration yields the value for the polarizability (α) of the barrier layer/solution interface at different temperatures.

- The dependence of the breakdown voltage on pH at constant [Cl^-] yields a value of -0.0109V for the dependence of the potential drop across the f/s interface, β. This value is similar to that measured for passivity breakdown of oxide barrier layers.

- The critical, areal cation vacancy concentration, ξ, leading to passivity breakdown on copper is in the range of 1.04×10^{15} - $1.14\times10^{15}cm^{-2}$ when temperature changes from 42 to 82 ℃, as determined from the dependence of the apparent breakdown potential on the potential sweep rate, as given by the PDM. These values are in excellent agreement with that (10^{14} - $10^{15}cm^{-2}$) estimated structurally, assuming vacancy condensation on either the copper substrate or on the cation sublattice of the barrier layer (Cu_2S).

- The experimentally-determined, near normal distributions in the breakdown potential for different temperatures are found to be in satisfactory agreement with theory in the quantitative characterization of the breakdown potential distributions for Cu as predicted from the PDM.

- Preliminary analysis shows that conditions that will be conducive to passivity breakdown and possibly stable pitting

will exist within the repository, particularly during the thermal phase and if the chloride concentration is high. In general, the pitting potential shifts to more negative values (pitting becomes more prevalent) with increasing [Cl^-] and with increasing temperature.

- Preliminary measurements have been made of the maximum pit depth from which the pitting factor is estimated, knowing the passive current density, and hence the general corrosion loss, just prior to pit nucleation. The passive current density is used to estimate the general corrosion metal loss using Faraday's law. The pitting factor (PF) is found to decrease exponentially with time, but it eventually levels off to a value between 4 and 14, depending upon the temperature (the PF is larger at higher temperatures). The maximum pit depth is found to approach a constant value with increasing time, as has been observed for many other systems, but the observation times were very short compared with the repository storage time, so that not too much significance must be read into these preliminary observations. However, they do illuminate the path that must be taken in future studies.

- We also report preliminary measurements of the repassivation potential and this parameter is found to decrease significantly with increasing charge passed during pit growth. We stress, however, that these pits are very shallow compared with those that may develop over the much longer times that will exist in the repository. The repassivation potential is expected to shift in the negative direction with increasing pit depth, such that a lower tendency will exist for active pits to die and the accumulation of localized corrosion damage to cease spontaneously.

- The pitting potential has been estimated for various times along the corrosion evolutionary path out to a horizon of 10,000 years by combining the predicted change in temperature with the dependence of the pitting potential as a function of temperature as measured in this work. The pitting potential is predicted to shift slightly in the negative direction (pitting becomes easier) during the initial heat-up of the repository followed by a long trend to more positive values (pitting becomes more difficult) as the temperature declines.

5.6. References

1. D. D. Macdonald and S. Sharifi-Asl, Is copper immune when in contact with water and aqueous solutions: Phase I, Research report 2011:09, Swedish Radiation Safety Authority, Sweden (2011).
2. D. D. Macdonald, S. Sharifi-Asl and G. R. Engelhardt, M. U. Macdonald, Issues in the corrosion of copper in a Swedish high level nuclear waste repository: Phase II, Research report 2012: 11, Swedish Radiation Safety Authority, Sweden (2012).
3. D. D. Macdonald, S. Sharifi-Asl, and G.R. Engelhardt, Issues in the Corrosion of Copper in a Swedish High Level Nuclear Waste Repository: Phase III. Role of Sulphide Ion in Anodic and Cathodic Processes, Technical Note 2014:57, Swedish Radiation Safety Authority, Sweden (2014).
4. F. X. Mao, C. F. Dong, S. Sharifi-Asl, P. Lu, and D. D. Macdonald, Passivity breakdown on copper: influence of chloride ion, Electrochim. Acta, 144 (2014) 391-399.
5. H. Andersson, F. Seitisleam, R. Sandström, Influence of phosphorous and sulphur as well as grain size on creep in pure copper, TR-99-39, SKB, Stockholm, Sweden (1999).
6. Long-term safety for KBS-3 repositories at Forsmark and Laxemar–a first evaluation. Main report of the SR-CAN project, Kärnbränslehantering, AB Svensk, 2009.
7. S. Sharifi-Asl, Ph.D. Thesis, Corrosion issues in high-level nuclear waste containers, The Pennsylvania State University, University Park, USA (2013).
8. M. G. Figueroa, R. C. Salvarezza, A. J. Arvia, The influence of temperature on the pitting corrosion of copper, Electrochim. Acta, 31(6) (1986) 665-669.
9. G. S. Frankel, N. Sridhar, Understanding localized corrosion, Materials Today, 11(10) (2008) 38-44.
10. N. G. Thompson and B. C. Syrett, Relationship between conventional pitting and protection potentials and a new, unique pitting Potential, Corrosion, 48(8) (1992) 649-659.
11. Anderko, N. Sridhar, M. A. Jakab, G. Tormoen, A general model for the repassivation potential as a function of multiple aqueous species. 2. Effect of oxyanions on localized corrosion of Fe–Ni–Cr–Mo–W–N alloys, Corros. Sci., 50 (2008) 3629-3647.
12. N. Sridhar and G. A. Cragnolino, Applicability of Repassivation Potential for Long-Term Prediction of Localized Corrosion of Alloy 825 and Type 316L Stainless Steel, Corrosion, 49 (11) (1993) 885-894.
13. S. Sharifi-Asl and D. D. Macdonald, Investigation of the kinetics and mechanism of the hydrogen evolution reaction on copper, J. Electrochem. Soc. 160 (6) (2013) H382-H391.

14. Y. Zhang, M. Urquidi-Macdonald, G. R. Engelhardt, D. D. Macdonald, Development of localized corrosion damage on low pressure turbine disks and blades: I. Passivity, Electrochim. Acta. 69 (2012) 1-11.
15. Y. Zhang, M. Urquidi-Macdonald, G. R. Engelhardt, Digby D. Macdonald, Development of localized corrosion damage on low pressure turbine disks and blades: II. Passivity breakdown, Electrochim. Acta, 69 (2012) 12-18
16. D. D. Macdonald, The point defect model for the passive state, J. Electrochem. Soc., 139(12) (1992) 3434-3449.
17. D. D. Macdonald, Passivity: The key to our metals-based civilization, Pure Appl. Chem., 71 (1999) 951-986.
18. D. D. Macdonald, The history of the Point Defect Model for the passive state: A brief review of film growth aspects, Electrochim. Acta, 56 (2011) 1761-1772.
19. G. Wranglen, Pitting and sulphide inclusions in steel, Corros. Sci., 14(5) (1974) 331-349.
20. G. S. Eklund, Initiation of pitting at sulphide inclusions in stainless steel, J. Electrochem. Soc., 121 (1974) 467-473.
21. R. C. Newman, H. S. Isaacs, and B. Alman, Effects of sulfur compounds on the chloride solutions, Corrosion, 38 (1982) 261-265.
22. P. Marcus, A. Teissier, and J. Oudar, The influence of sulphur on the dissolution and the passivation of a nickel-iron alloy - I. electrochemical and radiotracer, Corros. Sci., 24 (1984) 259-268.
23. D. D. Macdonald, D. F. Heaney, Effect of variable intensity ultraviolet radiation on passivity breakdown of AISI Type 304 stainless steel, Corros. Sci., 42 (2000) 1779-1799.
24. Y. Zhang, Ph.D. Thesis, Determination of damage functions for the pitting of AISI type 403 blade alloy and ASTM A470/471 disk alloy, The Pennsylvania State University, University Park, USA (2005).
25. R. Baboian and G. S. Haynes, Cyclic Polarization Measurements Experimental Procedures and Evaluation of Test Data, STP 727 Electrochem. Corros. Testing, (ASTM, Philadelphia, PA, 1981) 274-282.
26. K. J. Evans, L. L. Wong, R. B. Rebak, Determination of the Crevice Repassivation Potential of Alloy 22 by a Potentiodynamic-Galvanostatic-Potentiostatic Method, ASME/JSME 2004 Pressure Vessels and Piping Conference, (2004) 137-149.
27. N. G. Thompson and B. C. Syrett, Relationship between Conventional Pitting and Protection Potentials and a New Unique Pitting Potential. Corrosion, 48, 8 (1992) 649-659.
28. Anderko, N. Sridhar, D. S. Dunn, A general model for the repassivation potential as a function of multiple aqueous solution species, Corros. Sci., 46 (2004) 1583-1612.

6. Suggestions for future work

In Section 4.5, we have provided preliminary predictions of the evolution of localized corrosion damage on copper as the canisters transition along the corrosion evolutionary path (CEP). These predictions are "preliminary", because we do not yet have values of high fidelity for all of the parameters to determining the rate of evolution of the damage. Nevertheless, it is evident that conditions will exist in the repository, particularly during the initial thermal phase when the temperature is high, particularly if the chloride concentration is high under which passivity breakdown will occur and possibly under which macroscopic pitting damage will develop. However, these are many factors that must be considered when judging whether pitting will pose a threat to the integrity of the canister, including prompt repassivation constant, the kinetics of pit growth, delayed repassivation, the value of the repassivation potential compared with the passivity breakdown potential, and the corrosion potential, as the system transitions along the corrosion evolutionary path. These needs, and our recommendations for addressing them, are articulated below:

- The assumption that the electric field strength in a passive film is independent of the applied voltage and film thickness [1] needs to be demonstrated or denied experimentally. We are now convinced that this can be done using photo-electrochemical impedance spectroscopy (PEIS) and experiments would be initiated immediately in Phase V to explore this important issue. PEIS modulates the electric field via a modulated photon flux of super band-gap light onto a passive surface, with the impedance being defined as the vector ratio of the modulated light intensity and the resultant, modulated photo-current. This is a vitally-important issue, because it is central to the validity of Damage Function Analysis (DFA) [1], which is the protocol that will be used to predict the accumulation of damage as the canister transitions along the corrosion evolutionary path of the repository.
- We need to establish a more extensive database for passivity breakdown on copper in granitic groundwater by measuring the breakdown potential over a wider range of conditions and by measuring the survival probability (SP, the probability that a metastable pit will transition into a stable pit). The SP is

essentially the number of metastable pits that nucleate (and spontaneously repassivate) for every stable pit that nucleates and grows. Knowledge of this parameter is important, because the Point Defect Model predicts the rate of nucleation of meta-stable pits, not of stable pits. Thus, the rate of nucleation of stable pits, which result in macroscopic localized corrosion damage, is given by [1]:

$$\left(\frac{dn}{dt}\right)_{stable} = SP.\left(\frac{dn}{dt}\right)_{metastable} \qquad (5.1)$$

The value of the SP is determined by the ability of the newly-born pit nucleus to stabilize by establishing differential aeration, which, in turn, depends upon the ease with which the coupling current may be established between the pit nucleus and the external surface; this being necessary to feed resources from the external surface to the growing pit. The probability of establishing coupling between the pit nucleus and the external surface appears to be determined by the impedance to current flow through the porous corrosion product cap (remnant of the barrier layer) covering the pit nucleus, immediately after passivity breakdown.

- We need to measure and/or calculate the delayed repassivation constant for stable pits over realistic ranges in important system parameters. Delayed repassivation occurs when the external surfaces can no longer provide the resources in terms of the cathodic reaction (oxygen reduction and/or hydrogen evolution) that are required to maintain differential aeration. Separation of the local cathode (on the external surfaces) and the local anode (within the pit) results in the flow of a positive current (the "coupling current") through the solution from the pit to the external surface and in the flow of an electron current through the metal in the same direction. It is this current that maintains the aggressive environment within the pit and which maintains pit propagation. If this current is reduced below a critical value, the aggressive species that have accumulated within the pit disperse by diffusion into the bulk environment and the pit dies. Over the past three decades, we have developed sensitive methods for measuring the coupling current and these techniques will be used to mark when pit death occurs as a function of important variables, such as $[Cl^-]$, potential, pH, and temperature. The repassivation constant itself may be determined from the shape of the Integral Damage Function (IDF) for instantaneous nucleation

conditions (i.e., where att pits nucleate in a time that is short compared with the observation time). This will be the technique for determining the delayed repassivation constant that will be employed in any follow-on research.

- Whether pits will ultimately repassivate along the Corrosion Evolutionary Path (CEP) of the repository is determined by the relative values of the repassivation potential and the corrosion potential. The corrosion potential can be calculated with acceptable accuracy using mixed potential theory as we have described previously [2], but the repassivation potential is not currently amenable to theoretical prediction, because it is a sensitive function of pit depth and it is not feasible to grow pits "naturally" in the laboratory to depths that might be attained after exposure of the steel for thousands of years in the repository. Accurate measurement of the repassivation potential for realistic pit depths at simulated points along the CEP will require the use of artificial pits that are drilled into a metal surface to the desired depth. We will monitor the coupling current between the pit and an artificial cathode on the external surface to detect when differential aeration is fully developed and hence the artificial pit is behaving as a natural pit of much greater depth than can be realized in laboratory studies and then we will sweep the potential in the negative direction to determine the prepassivation potential from the polarization curve for the reverse sweep. These measurements could be made as a function of artificial pit depth and other independent variables (temperature, $[Cl^-]$, pH).

6.1. References

1. D. D. Macdonald and G. R. Engelhardt, Predictive Modeling of Corrosion, in: Richardson, J A et al (eds) Shreir's Corrosion, 2, pp. 1630-1679 (2010).
2. D. D. Macdonald, S. Sharifi-Asl, and G.R. Engelhardt, "Issues in the Corrosion of Copper in a Swedish High Level Nuclear Waste Repository: Phase III. Role of Sulphide Ion in Anodic and Cathodic Processes", Technical Note 2014:57, Swedish Radiation Safety Authority, Sweden (2014).

2016:30

The Swedish Radiation Safety Authority has a comprehensive responsibility to ensure that society is safe from the effects of radiation. The Authority works to achieve radiation safety in a number of areas: nuclear power, medical care as well as commercial products and services. The Authority also works to achieve protection from natural radiation and to increase the level of radiation safety internationally.

The Swedish Radiation Safety Authority works proactively and preventively to protect people and the environment from the harmful effects of radiation, now and in the future. The Authority issues regulations and supervises compliance, while also supporting research, providing training and information, and issuing advice. Often, activities involving radiation require licences issued by the Authority. The Swedish Radiation Safety Authority maintains emergency preparedness around the clock with the aim of limiting the aftermath of radiation accidents and the unintentional spreading of radioactive substances. The Authority participates in international co-operation in order to promote radiation safety and finances projects aiming to raise the level of radiation safety in certain Eastern European countries.

The Authority reports to the Ministry of the Environment and has around 300 employees with competencies in the fields of engineering, natural and behavioural sciences, law, economics and communications. We have received quality, environmental and working environment certification.

Strålsäkerhetsmyndigheten
Swedish Radiation Safety Authority

SE-171 16 Stockholm
Solna strandväg 96

Tel: +46 8 799 40 00
Fax: +46 8 799 40 10

E-mail: registrator@ssm.se
Web: stralsakerhetsmyndigheten.se